2021-02-24

Petrography and Geochemistry of Upper Paleozoic Sandstone around Kuch Area, Blue Nile Basin, Central Ethiopia: The implication for Provenance, Paleoclimate and Tectonic

Tigist Birhanu

Bahir Dar University

School of Earth Sciences

Department of Geology

Petrography and Geochemistry of Upper Paleozoic Sandstone around Kuch Area, Blue Nile Basin, Central Ethiopia: The implication for Provenance, Paleoclimate and Tectonic Setting

By

Tigist Birhanu

A Thesis Submitted to the School of Earth Sciences, Bahir Dar University in partial fulfillment of the Degree of Master of Sciences in Petrology

October, 2020

Bahir-Dar, Ethiopia

Approval of the thesis for defense

I hereby confirm that I have supervised, read, and evaluated this thesis/dissertation titled €Petrography and Geochemistry of upper Paleozoic Sandstone around Kuch Area, Blue Nile Basin, Central Ethiopia: the implication for Provenance, Paleoclimate and Tectonic Setting• by Tigist Birhanu prepared under my guidance. I recommend the thesis/dissertation be submitted for oral defense (mock-viva and viva voce).

Advisor,s name	Signature	Date

Approval of Dissertation/thesis for defense result

We hereby certify that we have examined this dissertation/thesis entitled €Petrography and Geochemistry of upper Paleozoic Sandstone around Kuch Area, Blue Nile Basin, Central Ethiopia: the implication for Provenance, Paleoclimate and Tectonic Setting• by Tigist Birhanu We recommend that Tigist Birhanu is approved for the degree of €Master of Sciences in Petrology•

Board of Examiners

______________	______________	______________
External examiner,s name	Signature	Date
______________	______________	______________
Internal examiner,s name	Signature	Date
______________	______________	______________
Chair person,s name	Signature	Date

Declaration

I hereby certify that the entire work to this thesis entitled €Petrography and Geochemistry of upper Paleozoic Sandstone around Kuch Area, Blue Nile Basin, Central Ethiopia: the implication for Provenance, Paleoclimate and Tectonic Setting• was done by me, Tigist Birhanu, for partial fulfillment of the requirements for the award of the Degree of Master of Science in petrology to the School of Earth Sciences, Bahir Dar University (BDU), under the supervision of Minyahl Teferi (PhD.) and Dawit Libene (PhD.).

I announce that the entire material is my original work and only with the use of the referenced literature and the described methods. The results embodied in this thesis have not been submitted in part or whole to any other university or institute for assessment or award of another degree.

ƒƒƒƒƒƒƒƒƒƒƒƒƒ ƒƒƒƒƒƒ.. ƒƒƒƒƒƒƒƒƒƒƒ

Name Signature date

ACKNOWLEDGMENT

First and for most I would like to thank the almighty for his absolute love and mercy, and for giving me the opportunity, strength and ability to undertake and complete this research.

Many individuals and organizations have contributed to this thesis that braved, supported, and stuck with me till the end of the thesis. My expensive and respectful gratitude goes first to my advisors; Dr. Minyahil Teferi and Dr. Dawit Libene, for their supportive guidance and motivation advice that help me a lot to challenge and explore new knowledge throughout this thesis.

During my field work, I received enormous assistance and care from the society of the Kuch area, for which I am very appreciative. Because of you, I accomplished my field work without any worry.

I also want to express my sincere thanks to BDU and WU Earth Science stuffs BDU laboratory assistants, and my colleagues for their encouragement, tough questions, constructive comments and suggestions. They were allowing me to experience what I have experienced.

I am indebted to my family and best friends who have always been for me no matter what, and for their unconditional support, motivation.

ABSTRACT

Paleozoic sedimentary rocks in the Blue Nile of central Ethiopia are related to two major Gondwana glaciations: namely, the Late Ordovician-Silurian and the Carboniferous-Permian glaciation. The present study investigates sandstone sections cropping out in the Bokotabo-Sentom and Daguja town, both of which are found around the Kuch area, in the western parts of Blue Nile basin, central Ethiopia. The upper Paleozoic sandstones are composed of mudstones, siltstones, and sandstones in the Bokotabo-Sentom area and deposited as sandstone, siltstone and tillite in the Daguja area. The present study is aimed at investigating the petrography and geochemistry of these sandstones to evaluate the provenance, the tectonic setting, and the paleoclimate conditions under which the upper Paleozoic sandstones were deposited. The study was conducted using a transmitted microscope, inductively coupled plasma mass spectrometry (ICP-MS), and inductively coupled plasma atomic emission spectroscopy (ICP-AES). Based on major, trace and rare earth element analysis and petrographic data, the upper Paleozoic sandstones are dominated by Quartz (on average of 64.5% in Bokotabo-Sentom area and 58.4% in Daguja area) and followed by feldspars (on average of 31.0% in Bokotabo-Sentom area and 36.6% in Daguja area) and rock fragment (on average of 3.2% in Bokotabo-Sentom area and 4.9% in Daguja area). The sandstone is medium to coarse-grained, texturally immature to sub-mature, and poorly to moderately sorted. The sandstone was derived from transitional continental and basement uplift rocks. The sandstone could be classified as arkose and lithicarenite. The chemical index of alteration, plagioclase index of alteration, and chemical index of weathering values identify the upper Paleozoic sandstone has moderate to high weathering history in the Bokotabo-Sentom area and low to moderate in the Daguja area. Based on trace and rare earth element concentrations, its sources possibly are juvenile material, the basement nearby.

Keywords: upper Paleozoic, Sandstone, Blue Nile basin, Petrography, Geochemistry, Provenance

Table of Contents

Approval of thesis for defense II
Approval of Dissertation/thesis for defense result III
Declaration IV
ACKNOWLEDGMENT V
ABSTRACT VI
LIST OF FIGURES IX
LIST OF TABLE X
ACRONYMS XI
1. INTRODUCTION 1
1.1. BACKGROUND OF THE STUDY 1
1.2. Location and accessibility 2
1.2.1. Physiography 3
1.3. Previous work 4
1.4. Statement of the Problem 5
1.5. Objectives 6
1.5.1. General Objective 6
1.5.2 Specific Objectives 6
1.6. Methodology 7
1.6.1 Field methods 7
1.6.2. Laboratory methods 7
1.7. Expected Outcome and Significance of the Study 11
2. REGIONAL GEOLOGICAL SETTING 12
2.1. Introduction 12
2.2. Stratigraphy of the Blue Nile Basin 12

2.2.1. The Precambrian basement 13
2.2.2. Palaeozoic sedimentary sussesions (pre-Adigrat sandstone) 13
2.2.3. Mesozoic sedimentary successions 14
3. GEOLOGY OF THE STUDY AREA 16
3.1. The Bokotabe-Sentom area 16
The sandstone units 16
The siltstone units 16
The mudstone unit 17
The upper sandstone 17
3.2. The Daguja area 19
The tillite unit 19
The sandstone-siltstone unit 19
4. PETROGRAPHIC AND GEOCHEMICAL RESULTS 22
4.1 Petrography 22
4.1.1 Bokotabo-Sentom area 22
4.1.2. The Daguja area 23
4.2. Geochemistry 27
4.2.1. Source rock compositions 27
4.2.2. Paleoclimate condition 41
4.2.3 Tectonic setting 44
5. DISCUSSION 47
5.1. Implications for provenance 47
5.2. Implications for paleoclimate 51
5.3. Implications for tectonic setting 53
Comparssion of the upper Paleozoic sandstone in Blue Nile Basin and Mekele Basin 55

6. CONCLUSIONS AND RECOMENDATION 56
Recommendation 56
References 57
Appendix 65

LIST OF FIGURES

Figure 1- (A) The geological map of Ethiopia; (B) Location Map of the study area 3
Figure 2- Physiographic map of the study area, ... 4
Figure 3- The flow chart showing the methodology of this thesis work 10
Figure 4- The outcrops view of sandstone units 18
Figure 5- Field photographs of the outcrops from Daguja area 20
Figure 6 (A) Geological map and lithostratigraphic column of Bokota-Sontom and Daguja area 21
Figure 7- Photomicrographs of the upper Paleozoic sandstones 25
Figure 8 - Multiple plots of all major elements against Al_2O_3 29
Figure 9 - (A) The selected major and trace element concentrations. (B) Rare-earth element concentrations 32
Figure 10 - Multiple plots of Al_2O_3 against all major elements in the Daguja area 34
Figure 11- (A) The selected major and trace element concentrations. (B) Rare-earth element concentrations 36
Figure 12- Geochemical classification 38
Figure 13 – (A) The Al_2O_3/TiO_2 vs. (SiO_2) digram (B) Ternary Ni – V – Th*10 diagrams 40
Figure 14 - A – CN – K ternary diagram [Al_2O_3 - (CaO*+Na_2O) – K_2O] 43
Figure 15- Chemical maturity of the upper Paleozoic sandstone 43
Figure 16- Tectonic discriminant function diagrams for the upper Paleozoic Sandstone 46
Figure 17- Tectonic setting discrimination diagrams based on major oxides 46
Figure 18- The QFL triangular diagram shows the classification of the upper Paleozoic sandstones 48
Figure 19- The QFL and QmFLt ternary diagram for tectonic discrimination 53

LIST OF TABLE

Table 1 Chemical classification of the upper Paleozoic sandstones based on (Lindesy, 1999)................37

Table 2- Locations of the upper Paleozoic sandstones sampling sites and outcrops..............................65

Table 3 Point-counted data and the derived QFL indices of the upper Paleozoic sandstone...................65

Table 4- Major element composition with CIA, CIW, and PIA values of Late Palaeozoic sandstones......66

Table 5- Trace elements composition of Late Palaeozoic sandstones...66

Table 6- Values of Pearson,s coefficient of correlation of major elements of the studied samples..........67

Table 7- Values of Pearson,s coefficient of correlation of the selected trace element...........................68

Table 8- Selected ratios for the upper Paleozoic sandstones...68

Table 9- Linear correlation coefficients for selected element distribution in the analyzed samples.........69

ACRONYMS

ACM „ active continental margin

Afsp „ alkali feldspar

ALS „ Australia laboratory service

ANS „ Arabian-Nubian Shield

CIA „ chemical index of alteration

CIW „ Chemical Index of Weathering

DF „ discriminant function

Gr „ granitoid

HFSE „ high field strength elements

ICP-AES „ inductively coupled plasma atomic emission spectroscopy

ICP-MS „ inductively coupled plasma mass spectrometry

IRF „ Igneous rock fragment

LILE „ large-ion lithophile elements

LOI „ Loss on ignition

MRF „ Metamorphic rock fragment

Mc „ microcline

Md „ mudstone (for thin section)

MST- mudstone (for thin section)

PAAS „ Post-Archean Australian Shale

PIA „ plagioclase index of alteration

Plg „ plagioclase

PM „ passive margin

QFL- Quartz- Feldspar- Lithics

Qm- monocrystalline quartz

QmFLt „ monocrystalline quartz-feldspar-lithic fragment

Qp- polycrystalline quartz

REE „ rare earth element (HREE„ heavy REE; LREE„ light REE)

Pl- Paleozoic

SIT „ siltstone

SRF „ Sedimentary rock fragment

SST „ sandstone

TIL „ tillites

TTE „ transition trace elements

UCC „ Upper Continental Crust

1. INTRODUCTION

1.1. BACKGROUND OF THE STUDY

In the Paleozoic, two main glaciation events have been reported from various locations within the Gondwana continent. However, the period and the areal coverage of the glaciated areas are not completely understood (Lewin et al., 2018; Elhebiry et al., 2019). The lower Paleozoic (upper Ordovician - Silurian) glaciation was depicted, relatively, as a limited, momentary (1-10 Ma) Hirnantian events and the upper Paleozoic (Carboniferous - Permian event) lasted for tens of millions of years (>70 Ma) (Isbell et al. 2012). During the Ordovician glaciation, a wide range of glacial deposits such as subglacial landforms including tunnel valleys, mega-scale glacial lineation, and paleo-ice streams have been formed, particularly in northern Gondwana (Armstrong et al., 2005). During the upper Paleozoic (Permo-Carboniferous) glaciation, the southwestward migration of the glaciogenic deposits was in response to movement of the southern pole across Gondwana from NW Africa to central Antarctica (Scotese and Barrett, 1990; Torsvik and Cocks, 2013). Both Paleozoic glaciations are identified in northern Central Africa (Niger and Chad), Horn of Africa (Eretria and Ethiopia) and southern Saudi Arabia, while Carboniferous-Permian glaciogenic deposits have been well documented from southern Arabia (i.e. Yemen and Oman) (Elhebiry et al., 2019). The upper Palaeozoic glacio-fluviatile and glacio-lacustrine deposits occur in East Africa (Wopfner and Kreuser, 1986). The upper Paleozoic silici- clastic sedimentary rocks are recognized from the south of the Equator, starting from Ethiopia in the north up to South Africa in the south (Elhebiry et al., 2019)

In Ethiopia, there are two types of Palaeozoic sedimentary rocks which are related to the two major Gondwana glaciations: Enticho sandstone (Late Ordovician to early Silurian) which is exposed in the Mekelle basin, and the upper Paleozoic sandstones (the Carboniferous, Permian) which are exposed in Mekelle basin (Edaga arbi glacials) and Blue Nile basins (Bussert, 2010; Lewin et al., 2018). They are underlain by Neoproterozoic basement rocks and overlain by Mesozoic clastic and carbonate sediments (Enkurie, 2010; Lewin et al., 2018).

The study area, Kuch area, is located in the Blue Nile Basin, central Ethiopia. The geological units that cover the Kuch area belong to the following three major categories: i) the Precambrian basement, ii) the Paleozoic-Mesozoic sediments, and iii) the Cenozoic Volcanic rocks (Tsige, 2008; Gani et al., 2009). The Paleozoic sedimentary rocks occur in the south and southeastern part of the study area, in the western parts Blue Nile basin (Dawit, 2014; Lewin et al., 2018). They are exposed in narrow zones and discontinuous bodies that have a generally south-north trend. The present study will cover two key areas, covering different parts of around Kuch area in the Blue Nile Basin: Bokotabo-Sentom and Daguja area.

The present study focused on the petrographic and geochemical characterization of the upper Paleozoic sandstone around the Kuch area, in the Blue Nile Basin, intending to provide insight into the provenance, paleoclimate, and tectonic setting. Petrographic and geochemical characterization of sediments is important for the implication of provenance, tectonic, setting and paleoclimate conditions. Thin sections were prepared at Geological Survey of Ethiopia, Addis Ababa, and then petrographic studies have been conducted using transmitted light microscopes in the petrology laboratory of the Department of Earth Science at Bahir Dar University. The analytical techniques for major, trace, and rare earth elements have been performed by inductively coupled plasma mass spectrometry (ICP-MS) and inductively coupled plasma atomic emission spectroscopy (ICP-AES) techniques at the laboratory of the ALS in Ireland. Other aspects such as textures are studied to the additional fulfill of the aim of the study.

1.2. Location and accessibility

The study area lies in the Northwestern plateau of Central Ethiopia and Southern parts of the Kuch area, bounded by $10^0$08,09•N to $10^0$24,45•N latitudes and between $37^0$00,44•E to $37^0$04,40•E longitudes overing a total area of 300 km^2. It is about 500 km far from Addis Ababa and is reached through two main routes. The first route is from Addis Ababa-Debre Markos,, Bure-Bokotabo road. The road from Addis Ababa to Bure is asphalted whereas a road from Bure to the study area is a gravel road. The other one is through Addis Ababa-Nekemte,, Agemsa - Bokotabo road. The road from Addis Ababa to Nekemte is asphalted and the remaining route from Nekemte to the study area is a gravel road. It is also accessed along with Bahir Dar-Debre Markos, Bure- Bokotabo road. The study area is accessible by a field car and motorcycle during all seasons.

Figure 1(A) The geological map of Ethiopia after (Billi, 2015); (B) Location Map of the study area, western Blue Nile basin, modified after (EMA, 1987).

1.2.1. Physiography

The physiography of the study area is characterized by subdued and rolling terrain dissected by streams which are tributaries of the Blue Nile River cross the area in a generally west-east direction in the central part of the area. The altitude within the study area ranges from about 1079 m to 2044m in the Bokotabo-Sentom area and 1200 to 1033m in the Daguja area. The study area, topographically, is characterized by valleys, flat area, and cliff with slope gradient varying from gentle to a steep slope.

Figure 2 Physiographic map of the study area, including both areas (Bokotabo-Sentom and Daguja area)

1.3. Previous work

The recent works that have been studied around the study area include Assefa (1991), Russo et al. (1994), Wolela (2007), Tsige (2008), Gani et al. (2009), Enkurie (2010), and Lewin et al. (2018). Assefa (1991) studied the lithostratigraphy and environment of deposition of the Late Jurassic-Early Cretaceous sequence of the central part of Northwestern Plateau, Ethiopia. Assefa studied lithostratigraphy and the depositional environment of the Mugher Mudstone and the Debre Libanos Sandstone of Northwestern Plateau. Russo et al. (1994) studied the sedimentary evolution of the Abay River (Blue Nile) Basin, Ethiopia. They gave a detailed explanation about the formation and evolutions of every succession in the Blue Nile basin which is; lower sandstone (Adigrat sandstone), Gohatsion formation, Antalo limestone, Mugher sandstone (muddy sandstone), and Debre Libanos sandstone (upper sandstone). Wolela (2007) studied the source rock potential of the Blue Nile (Abay) basin, Ethiopia. According to his study, the Permian Karroo Group shale was found to be over-maturing for oil generation; whereas algal-laminated gypsum from the Middle Hamanlei Limestone Formation was organic lean and had little source potential. Tsige (2008) studied and made the general Geological map and major structures of the Bure area. Gani et al. (2009) studied Stratigraphic and structural evolution of the Blue Nile Basin, Northwestern Ethiopian Plateau. They outlined the stratigraphic and structural evolution of the Blue Nile Basin based on field and remote sensing studies. Enkurie (2010) studied Stratigraphy, Facies, Depositional environments, and palynology of Adigrat sandstone in Northern and Central Ethiopia. He gave a detailed investigation of the stratigraphy, sedimentary facies, depositional environments, and palynology of the ‡Adigrat Sandstone, succession in the Mekelle and Blue Nile basins. Lewin et al. (2018) studied the Provenance of Paleozoic sandstones in Ethiopia, including the study area. They used petrographic and geochemistry – (X ray …uorescence) analysis to determine the provenance of the sandstone. According to Lewin et al. (2018), the upper Paleozoic sandstone is less mature with a geochemical signature of the more juvenile source material, most likely the Arabian, Nubian Shield. However, they only studied one sample from the upper Paleozoic sandstones of the Blue Nile basin.

1.4. Statement of the Problem

Even though the petrography and geochemistry of all sedimentary succession in the Blue Nile basin are well studied by the above authors, no detailed work has been done on the Paleozoic sandstone. General geology and major structures of the sandstone investigated by the Geological Survey of Ethiopia. Besides, Lewin et al. (2018) studied the Provenance of the upper Paleozoic sandstones in Ethiopia, but their study more focused on Northern Ethiopia, and only one sample was prepared in the Blue Nile basin. Hence, its geochemistry and petrography that reveal the provenance, paleoclimate, and tectonic setting of this sandstone have not been well studied yet.

Therefore, petrographical and geochemical studies are acquired to address the provenance, Paleoclimate, tectonic setting of the upper Paleozoic sandstone. Furthermore, structures and textures will provide adequate information about the depositional environments of the upper Paleozoic sandstones.

1.5. Objectives

1.5.1. General Objective

The general objective of the present study is to conduct petrographical and geochemical investigation on the upper Paleozoic sandstone around the Kuch area, the Blue Nile basin, Central Ethiopia, to evaluate the provenance, tectonic setting, and paleoclimate during the upper Carboniferous, Early Permian glaciation.

1.5.2 Specific Objectives

The specific objectives of the present study include:

- conducting a detailed petrographical investigation to determine the provenance of the upper Paleozoic sandstone;
- conducting detailed geochemical analysis (i.e., major, rare and trace element analysis) to calculate geochemical proxies, such as Chemical Index of Alteration (CIA), Plagioclase Index of Alteration (PIA), and Chemical Index of Weathering (CIW);
- assessing the paleoclimate and tectonic setting during the upper Carboniferous, lower Permian glaciations by using the calculated geochemical proxies;
- Attempting to conduct regional correlation with coeval deposits in Mekelle basin, in Ethiopia.

1.6. Methodology

Based on the availability and relevance, different methods and techniques are employed to accomplish the above-mentioned objectives.

1.6.1 Field methods

Forty-eight samples were collected from each lithological unit for petrographical and geochemical investigations. Two field trips were carried out during this study to examine the upper Paleozoic sandstone succession in the study area. The first field trip was conducted on December 25-31, 2019 for 6 days to observe and select well-exposed lithology and stratigraphic sections around the Bokotabo-Sentom area. The second field trip was conducted on January 11-14, 2020 for 4 days around the Daguja area to observe and select well-exposed lithology and stratigraphic sections. Geological traverses and orientations in the field were carried out by Bure topographic maps of 1:50,000 scales produced by the Ethiopian Mapping Agency. During the fieldwork, various sedimentary structures and textures; grain-size and color variations; mineral composition were examined. At the field, grains size was determined by hand-lens, and locations and thicknesses of each lithologic section were measured by GPS instrument.

Sample collection techniques

Forty-eight representative samples were collected based on sampling intervals that vary from 1 m to 15 m for each succession with little or no lithologic changes. 1-3 m sampling intervals were selected for lithology that rapidly changed. 25 (twenty-five) sandstones, 9 (nine) mudstones, 6 (six) siltstones, and 5 (five) tillites were collected from various sections for petrographic and geochemical analysis. These samples were labeled as SST for sandstone; SIT for siltstone; MST for mudstone; TIL for tillites; and Gr for granitoid. Field photographs and sketches were employed to document and illustrate key geological features such as sedimentary lithologies, structures, textures, and changes in exposure.

1.6.2. Laboratory methods

The analyses were done and emphasizing the petrographical and geochemical aspects of the observed rocks. The collected fresh samples were placed into zip lock polythene bags marked with sample number and location and sent to the Geological Survey of Ethiopia, Addis Ababa for thin section preparation and the laboratory of ALS for Geochemistry.

1.6.2.1 Petrographic analysis

The petrographic analysis is used for the determination of modal composition and textures of sandstones and it gives insight into the source material and the processes involved in the formation of the rock (Aleali et al., 2013). 17 (seventeen) samples which include; 11 (eleven) sandstones, 4 (four) siltstones, 1 (one) mudstone, and one tillite are prepared for thin section. The selected samples were sent for thin section preparation at the Geological Survey of Ethiopia, Addis Ababa. They were evenly cut into rectangular slabs and either side being polished for soft, flat surface then adherence to glass specimen plates. Later than, the sample slabs were trimmed and polished to get an even surface (~0.03mm thickness) that allowing maximum light distribution through the specimen plates. 17 (seventeen) thin-sections were prepared and analyzed by using a petrographic microscope. Then petrographic studies were conducted using polarized transmitted light microscopes in the mineralogy and petrology laboratory of the Department of Earth Science at Bahir Dar University. Rock compositions, grain-size, degree of sorting and roundness, and other features were studied. The modal analyses were carried out by counting more than 300 points per thin section, using the Gazzi-Dickinson point-counting method (Gazzi, 1966; Dickinson, 1970). After that, rooted in the modal composition, sandstone classification was made using the McBride scheme (McBride, 1963). Sandstone composition and tectonic discrimination were recognized by QFL and QmFLt plots proposed by Dickinson and Suczek (1979).

1.6.2.2 Geochemical analysis

Out of the 17 (seventeen) rock samples, 8 (eight) representative samples were selected for geochemical analysis. These samples are 3 (three) sandstones, 3 (three) siltstones, 1 (one) mudstone, and one tillite. The analytical techniques for major, trace, and rare earth elements has been performed by inductively coupled plasma mass spectrometry (ICP-MS) and inductively coupled plasma-atomic emission spectroscopy (ICP-AES) techniques. Before, weathered part of the samples removed; split into significant sizes, and the samples has been carefully crushed to chips of micron-size particles. They were crushed to 76.9% less than 2mm, ruffle split off 0.75g and then pulverized split to 91.4% passing 75µm before analysis. This preparation is done in ALS services plc, Nifas silk sub-city. These pulp samples were analyzed by ICP-AES for major oxides together with trace elements analyzed by ICP-AES and ICP-MS. These analyses were performed at the laboratory of the ALS Loughrea located at Dublin Road, Loughrea, Co. Galway, Ireland. The process was accomplished by dissolution of the pulp samples by lithium metaborate or tetraborate ($LiBO_2/Li_2B_4O_7$) fusion method. This mixing lithium metaborate or tetraborate fusion with a prepared sample (0.75g) was fused in a furnace at 1000°C. After that, an acid mixture (nitric, hydrochloric, and hydrofluoric acids) was used to cool and dissolve the mixture. The solution was then analyzed by ICP-AES and ICP-MS. For samples that are high in sulfides, a Na_2O_2 fusion may be substituted to obtain better result. Loss of ignition (LOI) represents the total volatile content of the rock that is determined by igniting the rock. It was measured after heating the samples overnight at 100ºC to remove water, at 550ºC for four hours to remove organic matter, and at 1000ºC for two hours to remove carbonates. The major and trace element concentrations were recalculated to 100% volatile free.

After geochemical analysis, the A-CN-K diagram, the CIA, CIW, and PIA, and elemental ratios were calculated to quantitatively measure the source rock composition and degree of weathering. The relative mobility of certain oxides has helped many researchers in developing some paleoclimate proxies such as the Chemical Index of Alteration (CIA), Plagioclase Index of Alteration (PIA), Chemical Index of Weathering (CIW), A-CN-K ternary diagram, and elemental ratios. In this study, these paleoclimate proxies were approved. Besides, the pattern of REE may give some indication of the weathering intensity. Correspondingly, the pattern of REE, major and minor element abundance, and their ratios have been used for the interpretation of the provenance. Bivariate, ternary, and multiple plots have been created by using the Geochemical Data toolkit (GCDkit) (Janoušek et al., 2006).

1.6.2.3 Summary of petrographic and geochemical methods

No	Analysis methods	No of samples	Examination
1	Petrographic analysis	17	Modal and source rock composition a texture
2	Geochemical analysis (ICP-AES and ICP-MS)	8	trace and major element for discrimination tectonic setting and provenance

Figure 3- The flow chart showing the methodology of this thesis work

1.7. Expected Outcome and Significance of the Study

The outcome of this thesis work will to contribute the understanding of the provenance, tectonic setting and paleoclimate of the upper Paleozoic sandstone in the Bure area, Western part of Blue Nile basin, Central Ethiopia. Additionally, the output will be;

- a detailed petrographical investigation that determines the provenance of the upper Paleozoic sandstone;
- detailed geochemical analysis (i.e., major, rare, and trace element analysis) that calculate geochemical proxies;
- a detailed evaluation of the paleoclimate and tectonic setting during the upper Carboniferous, lower Permian glaciations by using the calculated geochemical proxies;
- Regional correlation with coeval deposits in Mekelle basin, in Ethiopia.

The Significances of this research is to give comprehensive information on the provenance, tectonic setting, paleoclimate, and depositional condition of the upper Paleozoic sandstone around the Kuch area, western Blue Nile Basin.

2. REGIONAL GEOLOGICAL SETTING

2.1. Introduction

The final assemblage of Gondwana was an extended process during the Neoproterozoic between 650 Ma to 600 Ma. During this time, the East African Orogen was formed which is one of the largest accretionary orogens in Earth's history (Collins and Pisarevsky, 2005; Abate et al., 2015). At the end of the Precambrian time the accretion and dismantle of the East African Orogen occurred, which was followed by a long period of erosion (Mogessie et al., 2002; Dawit, 2014). In Northern Africa, a vast peneplain developed after the consolidation of the newly formed continent, on which a blanket of Paleozoic sandstone was deposited (Avigad et al., 2005). Between Paleozoic and Triassic, the Precambrian tectonic structures reactivated as extensional faults that guide the deposition of eolian and glacial deposits (Edaga Arbi Glacials and Enticho Sandstones), and successively of alluvial plain sediments (Adigrat Sandstones) (Dawit, 2014; Abate ea al., 2015 and Sembroni et al., 2016). From three major transgression and regression cycles, the first cycle was responsible for the formation of the majority of Mesozoic sediments in Ethiopia (Kazmin, 1972; Mogesse et al., 2002). In Cenozoic, around Eocene, the impingement of the Afar plume starts to deform the lithosphere causing a regional broad uplift and the emplacement of the flood basalts on the Paleo-Mesozoic sandstone (Dawit, 2014; Sembroni et al., 2016).

2.2. Stratigraphy of the Blue Nile Basin

The Blue Nile Basin is situated in the northwestern Ethiopian plateau, between latitudes 08˚45' to 10˚30' N and longitudes 36˚30' to 39˚00' E and covers an area of 55,000 square kilometers (Enkurie, 2010). It is one of a series of NE and NW-trending intra-continental rifts and extensional basins, which were subsequently filled with about 2000 meter section of Paleozoic-Mesozoic sediments (Mogessie et al., 2002; Gani et al., 2009). The stratigraphy of the Blue Nile Basin is characterized by the Precambrian crystalline basement, Palaeozoic and Mesozoic sedimentary successions, and the Tertiary continental flood basalts (Trap series). Paleozoic-Mesozoic sedimentary rocks unconformably overlying on the Neoproterozoic basement rocks and unconformably overlain by Early-Late Oligocene and Quaternary volcanic rocks (Gani et al., 2009).

2.2.1. The Precambrian basement

The Neoproterozoic basement rock, ranging from 850 to 550 Ma, lies on the base of the Paleozoic–Mesozoic sedimentary succession in the Blue Nile Basin (Gani et al, 2009; Enkurie, 2010). It consists of low-grade meta-volcano-sedimentary succession and mafic-ultramafic complexes of the Arabian Nubian Shield (ANS) and the high-grade metamorphosed and deformed Mozambique Belt (MB), produced between West and East Gondwana by the closure of the Mozambique Ocean (Tadesse et al. 2000; Stern et al. 2004). These are overlain unconformably by a Permo-Triassic "Karroo" succession around 450 m thick (Wolela, 1997).

2.2.2. Paleozoic sedimentary successions (pre-Adigrat sandstone)

The Palaeozoic units comprise sediments of one of the two major Gondwana glaciations, Late Carboniferous to Early Permian glacial-fluvio/ lacustrine deposits (Bussert and Schrank, 2007; Bussert, 2010). According to (Russo et al., 1994), Pre-Adigrat sediments are considered as a single unit, but after (Enkurie, 2010), Paleozoic sedimentary rocks are classified into three sections: Pre-Adigrat I, Pre-Adigrat II, and Pre-Adigrat III sediments

2.2.2.1. Pre-Adigrat I

Pre-Adigrat I sediments are the oldest sedimentary succession in the Blue Nile basin with a thickness of up to 50 m (Enkurie, 2010). This rock is composed of poorly sorted, massive to crossbedded medium- to coarse-grained white sandstones and conglomerates (Enkurie, 2010). Different structures such as ductile soft-sediment deformation structures, large-scale trough crossbedding, crude horizontal bedding, and channel-type cut and fill structures have been found (Enkurie, 2010). These structures lead to correlate this succession with the lower glaciogenic part of the Enticho Sandstone in northern Ethiopia. It overlies the crystalline basement and is exposed in small isolated outcrops (Enkurie, 2010).

2.2.2.2. Pre-Adigrat II

Pre-Adigrat II sediments are extensively exposed in the Blue Nile basin and reach a maximum thickness of 400 m in the Fincha valley of central Ethiopia and it reaches up to 200 m in the northwest of Blue Nile basin (in Bokotabo area, which is the parts of the study) (Enkurie, 2010). These successions are composed of lateral accretion deposits, floodplain fines, crevasse splays, playa-lake, and eolian dune sediments (Dawit and Bussert, 2009; Enkurie, 2010). Based on the age of the overlying unit, the age of these succession is considered to be pre-late carboniferous. It is unconformably overlain either pre-Adigrat I or the Precambrian basement (Enkurie, 2010).

2.2.2.3. Pre-Adigrat III

Pre-Adigrat III sediments have a thickness of 350 m in Fincha and Dedu areas and 100 m in Fuliya and Dejen areas (Enkurie, 2010). It consists of three successive cycles of stacked, multi-story sheet sandstone bodies that are capped by overbank fines and crevasse splay deposits. These successions can be interrelated with Karoo sediments (fluvial and lacustrine syn-rift sediments) which are widespread in eastern and southern Africa (Enkurie, 2010). Based on palynological dating, the lower part of these successions are late Carboniferous to Early Permian age (which is also the parts of the study) (Price, 1983; Stephenson et al., 2003), and the top of the succession indicate a Middle Triassic age (Geletu & Wille 1998). These successions are underlain by Pre-Adigrat sediments and overlain by Adigrat sandstone (Enkurie, 2010).

2.2.3. Mesozoic sedimentary successions

2.2.3.1. Adigrat sandstone

Adigrat Sandstones have a thickness of ~300 m and deposited above the partially peneplain Triassic surface that is unconformably developed above the Permo-Triassic sediments as well as of the basement and overlain by an Early–Middle Jurassic Lower Limestone unit (Gani et al., 2009; Abbate et al., 2015). Based on some biostratigraphic data and correlation with adjacent areas that providing fossil ages, this succession is assigned as Triassic–Early Jurassic in age (Russo et al., 1994).

2.2.3.2. Gohatsion formation

The succession has a thickness of 450 m and It is assigned as Early–Middle Jurassic age (Toarcian to Bathonian) (Assefa, 1981). It consists of a cyclic repetition of facies successions that are composed of alternating dolostones, marlstones and shales, bioturbated mudstones with thin siltstone intercalations, fine-grained coquinoid cross-laminated sandstones, and thick beds of gypsum (Assefa, 1981; Russo et al., 1994). It is underlain by the Adigrat sandstone unit and overlain by a Middle-Late Jurassic Antalo Limestone unit (Gani et al., 2009).

2.2.3.3. Antalo Limestone

This unit is a carbonate succession of the Middle-Late Jurassic age, based on the Callovian to Kimmeridgian benthic foraminifers and macrofaunas (Russo et al. 1994 and Atnafu, 2003). It is found in the SW…owing segment of the Blue Nile basin, which comprises thinly bedded to massive limestone with a thickness of ~400 m (Gani et al., 2009). This unit is sandwiched between the Gohatsion Formation and either the Mugher mudstone unit or the Debre Libanos Sandstone unit or the volcanic rocks (Gani et al., 2009; Enkurie, 2010).

2.2.3.4. Mugher Mudstone

This unit is named by Assefa (1991) after the unit was found alongside the Muger River in the eastern part of the Blue Nile basin. It is believed to post-Kimmeridgian to pre-Middle Eocene age based on stratigraphic position (Assefa, 1991). This unit is dominantly exposed in the canyons of Mugher, Ega, Wodem, Dersena, Beresssa, Adabai, Zhema, Wanchit, and Chennli rivers (Mogessie et al., 2002). It is conformably underlain by the Antalo Limestone and overlain by either the Debre Libanos Sandstone unit or the volcanic rocks (Enkurie, 2010).

2.2.3.5. Debre Libanos Sandstone

Its thickness varies from west to east; from ~200 up to ~500 m with average thickness of 280 m (Gani et al., 2009; Enkurie, 2010). Based on its stratigraphic relationship with overlying and underlying units, its age is assigned to be of Late Jurassic „ Early Cretaceous age (Assefa, 1991; Russo et al., 1994). It is underlain by Mugher mudstones and unconformably overlain by the Early „ Late Oligocene volcanic rocks (Assefa, 1991; Gani et al., 2009 and Enkurie, 2010).

2.2.3.6. Trap series

The basalt series with subordinate trachytes and rhyolites envelop most of the Northwestern Ethiopian Plateau and overly the Debre Libanos sandstone or Antalo limestone, in place (Gani et al., 2009; Enkurie, 2010). Based on Arage dating and magneto-stratigraphy, these units are assigned as Lower „ Upper Oligocene age (26.9 „ 29.4 Ma) and vary in thickness from 500 to 2000 m (Hofmann et al., 1997).

3. GEOLOGY OF THE STUDY AREA

The studied area is bounded between $10^0$18,09•N to $10^0$24,45•N and $37^0$00,44•E to $37^0$04,40•E and are grouped into two sections; the Bokotabo-Sentom area and the Daguja area (fig-1).

3.1. The Bokotabo-Sentom area

The upper Paleozoic sandstone sections are located from the northeast of the Bokotabo village to the southeast of the Sentom village. It covers $10^0$22,55•N to $10^0$24,45•N and $37^0$00,44•E to $37^0$04,40•E. The upper Paleozoic sandstone sections in this area reach about 150m. It is unconformably underlain by the Neoproterozoic basement and unconformably overlain by Adigrat sandstone. This work categorizes the studied upper Paleozoic sandstone into three units based on lithology and mineralogical composition. This succession is composed of sandstone, siltstone, and mudstone unit.

The sandstone units

This sandstone unit is found at the bottom of the formation and exposed in the northeast of the Bokotabo area. This unit is unconformably underlain by Neo-Proterozoic granitoid rocks. It is approximately, 60m in thickness. This massive sandstone formation is fine to medium-grained, sub-angular to sub-round in shape, and moderately sorted with variable color (pale purple, white and red). This unit is mostly composed of quartz and feldspar minerals. At the bottom, this unit contains soft sandstone with cm-sized clasts (fig-4-E). The white sandstone is spotted by red color minerals which may indicate Fe-oxide minerals such as hematite. The pale-purple sandstone is relatively fine-grained in size. Some structures are observed in this section such that: graded bedding and trough cross-bedding (fig-4-B & C) which are also the characteristics of glacial sandstones. This sandstone unit is overlain by laminated siltstones.

The siltstone units

This laminated siltstones unit is approximately 04m in thickness. It has a white and red color (fig-4-D). The white siltstone intercalated with mudstone is mainly composed of fine quartz with some pinkish minerals which may be feldspar minerals. The red-colored siltstone may be due to Fe-oxide minerals. This formation is fine to medium grained and moderately sorted. It is overlain by laminated mudstone in the Sentom area and overlain by Adigrat sandstone in the Bokotabo area.

The mudstone unit

This mudstone unit is only exposed in the Sentom area and has roughly 50m thickness. It is entirely reddish which may indicate the composition is dominated by Fe-oxide minerals such as hematite, as cementing materials. Two types of mudstone are observed in this area. The upper part is highly laminated and friable, while the bottom one is hard and massive mudstone. This hard and massive mudstone overlies the siltstone in the Sentom area.

Adigrat sandstone

This sandstone is fine to coarse-grained, medium sorted with variable color (yellow, pure white and red sandstones). Its thickness reaches about 100m. Different structures are observed in this section; graded bedding, herringbone cross-bedding trough and planar-tabular cross-bedding, and hummocky cross-bedding (fig 4F&G). Tabular and herringbone cross-bedding are common in this unit. It is overlain the siltstone units in the Bokotabo area, and mudstones in the Sentom area.

A

B

C

D

E

F

G

Figure 4- The outcrops view of sandstone units and show (A) partial view of siltstone and mudstone units overlying by Adigrat sandstone, (B) and (C) the sandstone unit showing trough cross-bedding, (D) thin white and dark red laminated siltstone, (E) outsized clasts in sandstone, (F) herringbone cross-bedding, (G) hummocky cross-bedding.

3.2. The Daguja area

This area is bounded between $10^0$18,09•N to $10^0$19,49•N and $37^0$01,00•E to $37^0$03,10•E. The thickness of this section is approximately reached to 130 meters. It consists of two sections; the tillite and sandstone and siltstone section (fig-5-A).

The tillite unit

The tillite unit is unconformably underlain by Neo-Proterozoic granitoid rocks. Its thickness reaches up to 50m. It consists of rounded clasts with white and pinkish color (fig-5-D). The grain size of these clasts ranges from fine rocks to boulder size. Most of these clasts are granitoids. The matrixes in this unit have whitish-yellow color and medium to coarse grain size and sub-angular shape. This tillite is overlain by pale-yellow sandstone-siltstone unit.

The sandstone-siltstone unit

This massive sandstone-siltstone unit has a thickness reaches up to 80m. It has yellow and pale-yellow color (fig-5-B). The siltstone unit is hard and composed of fine yellowish grains. The sandstone unit is both soft and hard massive sandstone. It consists of fine to medium grains, sub-angular to sub-round in shape, and moderately sorted grains. Only normal graded bedding structure is observed in this unit (fig-5-C).

A

B

C

D

Figure 5- Field photographs of the outcrops from Daguja area (A) a partial view of tillite and sandstone in the study area, (B) a cliff showing massive yellow sandstone, (C) normal graded bedding in sandstone (D) tillite boulder outcrop that composed of medium to coarse-grained clasts

A geological map was prepared at a scale of 1:50,000, based on their lithologic change. The vertical exaggeration between the geological map and the cross-section is 1:1. A normal fault is found in the northwestern parts of the Bokotabo area. This fault dissects all sedimentary units (including Adigrat sandstone) except the upper Paleozoic sandstone which underlain the siltstone unit. A-B crosssection was chosen to show all lithological units. The upper Paleozoic sandstones in both areas are underlain by the Neoproterozoic granitic basement and overlain by Adigrat sandstone and tertiary basalt.

Figure 6 (A) Geological map and lithostratigraphic column of Bokotabo-Sentom and Daguja area with samples for petrography and geochemistry analyses; LP (late Paleozoic), M (Mesozoic). (B) Geologic cross-section of Bokotabo-Sentom and Daguja area.

4. PETROGRAPHIC AND GEOCHEMICAL RESULTS

4.1 Petrography

The mineralogical composition of the upper Paleozoic sandstones was determined by using Gazzi, Dickinson,s point-counting method and plotted in a QFL and QuFLt ternary diagram for sandstone classification tectonic setting discrimination (fig-18 & 19). Petrographic descriptions are presented in (Table-3). According to the classification scheme of McBride (1963), based on the modal composition the upper Paleozoic sandstone in both areas is dominated by arkose (fig-18).

4.1.1 Bokotabo-Sentom area

17 (seventeen) thin sections were prepared and analyzed under polarized microscope. The major constituent minerals in these samples are quartz, plagioclase, K-feldspar, the mica minerals (muscovite and biotite), carbonate (calcite), and accessory minerals (zircon, tourmaline, garnet, and FeTi oxide), respectively. Framework grain components dominate 87 vol. % of the rock samples with matrix and cement constitute about 13 vol. %. Based on the overall analysis, the upper Paleozoic sandstone has an average modal composition of 65.6 vol. % quartz, 30.1 vol. % feldspar, 3.7 vol. % lithic fragments and 0.5 vol. % accessory minerals. The samples' texture ranges from fine- to coarse-grained, sub-angular to sub-rounded, and moderately to poorly sorted sandstones (table-3). In the sampled thin section, the rock (lithic) fragments are composed of metamorphic, sedimentary, and plutonic rocks (fig-7E). In thin sections heavy minerals are dominated by zircon, tourmaline, rutile, garnet, iron oxides (magnetite, and hematite), few opaque phases, and minor orthopyroxene, while most of them have occurred as inclusions (fig-7 E & F). Grains of heavy minerals are very fine and rounded to well-rounded grains. All analyzed samples contain cement such as silica, calcite, and mica (fig-7J). Sandstone samples for instance Sst3-bok and Sst8-bok are strongly cemented with silica; Sst4-bok and Sst9-bok are strongly cemented with calcite and Sst12-bok is strongly cemented with hematite. In some samples, quartz, plagioclase, and some lithic fragments are altered to hematite and calcite. Sandstone samples (Sst5-bok, Sst6-sen, and Sst10-bok) are different from their compositions from the rest samples; they are related to Adigrat sandstones.

Quartz is the principal constituent mineral in the studied samples with three varieties; monocrystalline (Qm), polycrystalline (Qp), and stretched quartz (fig-7G). The quartz grains are generally sub-angular to sub-round in shape. Along with quartz grains, monocrystalline quartz is leading over polycrystalline quartz with an average modal volume percentage of 43.3 vol. % and 21.2 vol. %, respectively. The majority of the Qm grains show straight to slightly undulatory extinction and some quartz grains contain inclusions such as quartz, zircon, tourmaline, and garnet (fig- 7-A & H). Feldspar is the second most dominant constituent minerals with sub-angular shapes. Plagioclase, orthoclase, microcline, and perthite are the major common varieties, respectively (fig- 7-A&K). Plagioclase dominates over K-feldspar with the average modal composition of 23.4 vol. % and 4.1 vol. % respectively. Among K-feldspar, microcline is dominant over orthoclase and micro-perthite. Rock (lithic) fragments are the least framework grain with an average modal composition of 7.3 vol. %. In general, the fragments are sub-angular in shape. They are abundant with siltstone, metamorphic lithoclasts, and plutonic lithoclasts, respectively. Metamorphic lithoclasts are slates, schist, and meta-sedimentary rocks which show foliation (fig- 7-E&I). The sedimentary lithoclasts are fine sandstone and siltstones. Cementing materials occurring as pore fillings are composed of silica, carbonate (calcite), iron oxides (hematite), and mica (muscovite and biotite) minerals, respectively (fig- 7-I & J). Fluid, lithic fragment and heavy mineral inclusions are observed in the analyzed thin sections (fig- 7-A, E & H).

4.1.2. The Daguja area

The analyzed samples in this section have the major components of quartz (64 vol. %), feldspar (30.7 vol. %), lithic fragments (4.8 vol. %), and accessory minerals (0.5 vol. %). The samples vary from fine- to coarse-grained, sub-angular, and moderately to poorly sorted sandstones (Table-3). The lithic fragments are metamorphic, sedimentary, and plutonic in origin. Framework grain components account for 86 vol. % of the rock samples with matrix and cement constitute about 14 vol. %. Accessory minerals are zircon, tourmaline, rutile, garnet, Fe-oxides, and minor orthopyroxene (Table-3). Types of cement are silica, calcite, and mica (muscovite and biotite). Siltstones sample (Sit-1dag) is strongly cemented with calcite followed by muscovite, Sst1-dag strongly cemented with hematite and muscovite without any calcite cement. Sst2-dag and Sst3-dag are moderately cemented with silica, hematite with little calcite (fig- 7- I, J& K). The quartz grains are generally sub-angular to sub-round; monocrystalline (Qm) is dominated over polycrystalline (Qp) with an average of 40.5 vol. % and 23.5 vol. %, respectively (Table-3)

The majority of the Qm grains have undulatory extinction and some quartz grains contain mineral inclusions such as rutile, zircon, tourmaline, and garnet.

Feldspar is the second dominant constituent with sub-angular grains. Plagioclase, orthoclase, microcline, and micro-perthite are the major constituent minerals. Plagioclase dominates over K-feldspar (22.9 vol. % and 7.8 vol. %, respectively) (Table-3). Among K-feldspar, microcline is dominant over orthoclase minerals.

Rock (lithic) fragments are the least framework grain with an average of 4.9 vol. %. In general, the fragments are sub-angular in shape. They are abundant with plutonic lithoclasts, siltstone, claystone, and metamorphic lithoclasts respectively. Metamorphic lithoclasts are composed of slates, micaceous schist, and meta-sedimentary rocks. The sedimentary lithoclasts are sandstone and siltstones.

A B

C D

E F

Figure 7- Photomicrographs of the upper Paleozoic sandstones showing (A) and (B) monocrystalline and polycrystalline quartz (Qm and Qp), plagioclase and microcline (xpl and ppl, 4x); (C) and (D) mudstone, monocrystalline quartz and microcline (xpl and ppl, 4x); (E) and (F) mineral inclusion in kyanite (red, blue and black arrow), pore space(green arrow) (xpl and ppl, 10x)

G H

I J

K L

(G) monocrystalline and polycrystalline quartz with stretched grains cemented by silica with some hematite micro-crack on the quartz crystal (xpl, 10x); (H) monocrystalline quartz with inclusion(Qin) and undulatory extinction (Qu) (xpl, 10x); (I) cements such as calcite (Ca, yellow arrow), muscovite flakes (green arrow), biotite (red arrow) and hematite (blue arrow) (xpl, 4x); (J) cements hematite (green arrow),calcite (red arrow), and siltstone rock fragment (blue arrow), muscovite (yellow arrow) (xpl, 4x); (K) micro-perthite grains (xpl, 10x); (L) fluid inclusion in quartz (xpl, 4x).

4.2. Geochemistry

4.2.1. Source rock compositions

The major and trace element concentration and their ratios of all analyzed samples are given in (Table- 4&5). The sandstones were measured up to the average composition of the upper continental crust (UCC) (McLennan, 2001) and PAAS (Taylor and McLennan, 1985). The selected major and trace elements normalized to the primitive mantle (Sun & McDonough, 1989) are plotted in (fig- 9&11). Besides, REE data were plotted on REE primitive mantle spider plots (McDonough & Sun, 1995). The entire samples show comparable patterns with upper continental crust and Post-Archean sediments that display LREE enrichment and moderately HREE pattern (fig-9& 11).

4.2.1.1 Bokotabo-Sentomarea sandstone

8 (eight) samples were prepared and analyzed by inductively coupled plasma mass spectrometry (ICP-MS) for trace and rare earth elements and inductively coupled plasma-atomic emission spectroscopy (ICP-AES) techniques for major, trace, and rare earth elements. The SiO_2 content in this sample is an indicator of the abundance of all silicate minerals present in the sandstone mainly quartz, feldspars, and clay minerals, while quartz is the important mineral. It accounts for the highest concentrations in all samples (74, 96 wt. %). Other major elements are relatively have low concentration: Al_2O_3 (3- 14.05 wt. %, mean- 8.50 wt. %), Na_2O (0.01- 4.14 wt. %, mean 1.62 wt. %), Fe_2O_3 (0.41- 4.37 wt. %, mean 1.73 wt. %), K_2O (0.04- 2.01 wt. %, mean-0.93 wt. %), TiO_2 (0.11- 0.75 wt. %, mean 0.30 wt. %), CaO (0.02-0.67 wt. %, mean 0.23 wt. %), MgO (0.04- 0.49 wt. %, mean 0.18 wt. %), P_2O_5 (0.01- 0.18 wt. %, mean 0.05 wt. %), and MnO (0.01- 0.05 wt. %, mean 0.02 wt. %). Some samples from this area show nearly negligible concentrations of some major elements such as CaO, MnO, P_2O_5, and TiO_2. The ratios of SiO_2/ Al_2O_3 values are range from 5.31 to 32.00. All the studied samples show low CaO/ Al_2O_3 values (0.007 to 0.06). Moreover, the low concentrations of TiO_2 (<1wt. %) that show low abundances of Ti-bearing opaque minerals such as rutile. When compared with UCC (McLennan, 2001) PAAS (Taylor and McLennan, 1985) the studied samples are characterized by high SiO_2 contents and low in Al_2O_3, Fe_2O_3, CaO, Na_2O, MgO, K_2O. However, siltstones (SIT5 & SIT6) have a higher value of Na_2O than the UCC and PAAS. The depletion of Na_2O (< 1 wt.

%) in mudstone can be attributed to a relatively smaller amount of Na-rich plagioclase in them (Table-4). According to K_2O and Na_2O contents and their ratios, the mudstone sample has the highest ratio (K_2O/Na_2O =18). Al_2O_3 content is relatively high in all samples except sandstones sample # SST5 (3 wt. %). The sandstone sample (SST5) has the highest value of SiO_2 (96 wt. %), and it has the lowest value of other major oxides such as Al_2O_3, K_2O, Fe_2O_3, CaO, MgO, Na_2O. Depend on all geochemical value, the sandstone sample (SST5) might be different from other samples during their formation, it is possibly from Adigrat sandstone.

The correlation between SiO_2 and other major elements is negative for the studied samples that indicate much of the SiO_2 is present as quartz grains. The SiO_2 content of the studied samples shows a strong negative correlation with Al_2O_3, TiO_2, Fe_2O_3 and P_2O_5, and a weak negative correlation with MgO, Na_2O, and CaO (Table-6). Except for SiO_2, all major elements have a positive correlation with Al_2O_3 (fig-8); P_2O_5, Fe_2O_3, TiO_2, and K_2O strongly correlated, while Na_2O, MgO, and CaO weakly correlated, and MnO exhibit no correlation. Mudstone has, relatively, high concentration of TiO_2 that indicates Ti-rich opaque minerals such as rutile. Additionally, it has increased trace element concentrations (Th, Y, Zr, and REEs like Ce, Dy, Gd, La, Sm, and Tb), that indicate heavy minerals such as zircon (Table-5).

Figure 8 - Multiple plots of all major elements against Al_2O_3; (A) Al_2O_3 vs SiO_2, (B) Al_2O_3 vs CaO, (C) Al_2O_3 vs MgO, (D) Al_2O_3 vs Na_2O, (E) Al_2O_3 vs K_2O, (F) Al_2O_3 vs TiO_2, (G) Al_2O_3 vs P_2O_5, and (H) Al_2O_3 vs Fe_2O_3; all major elements are measured by w.%

Large-ion lithophile elements (Rb, Ba, Pb, Cs, and Sr) are relatively mobile and incompatible elements. Ba, Rb, Pb, Sr, Cs concentrations in all samples are well below the values for the UCC, except siltstone samples that are enriched in Ba compared to the UCC (fig-9A). These mobile elements are enriched in mudstone and siltstone than the sandstones. Cs, Rb, Sr and Ba show a strong positive correlation with Al_2O_3 (Table - 9). All studied samples are enriched in Pb that indicates arkosic sandstone, except sandstones (SST3 and SST5) which have negligible amount of Pb (< 2 for both samples).

High field strength elements (Th, U, Ti, Hf, Zr, Nb, and Ta) are incompatible and immobile elements that are enriched in felsic rather than mafic rocks (Bauluz et al., 2000). They are used as an indicator of provenance due to their immobility (Taylor and McLennan, 1985). All HFSE in the studied sample, except mudstone, are well below values for the UCC (fig-9-A). The studied mudstone shows higher concentrations of field high strength elements (HFSE) such as Zr, and Hf compared to UCC. The lower sandstone (SST3) shows depletion in high field strength elements such as Ga, Ta, Hf, Nb, Sm, Th, U, Zn, and Zr. The depletion of Hf (2.1-4.5 ppm) in all samples, except mudstone (9.1ppm) is due to the depletion of mafic minerals in them (Table-5). Th shows weak positive correlation with Al_2O_3 (r= 0.64471) and strong positive correlations with elements, such as TiO_2 and Nb (r = 0.985788 and r= 0.998344, respectively) (Table-7&9).

Transition trace elements (Sc, Cu, and Ni): All transition trace elements are depleted compared to the UCC (fig-9-A). Mudstone is relatively enriched by Cu and Sc, while Ni is enriched in siltstone. Medium correlations between Cu and Ni and selected major elements have been observed (Table-9). The depletion of Sc and Ni in all studied samples indicates the depletion of mafic rocks in these formations. Sc correlates strongly positive with Al_2O_3 (r=0.879816), TiO_2 (r=0.934036), Zr (r=0.884455) and the REEs (r=0.859301; r=0.915178 for HREEs) (Table-7&9).

Rare earth elements (La, Ce, Pr, Nd, Sm, Eu, Gd, Tb, Dy, Ho, Er, Yb and Lu) are the least concentration, insoluble, and relatively immobile element during weathering, and have the most important application for provenance in sedimentary rocks (McLennan, 1989; Rollinson, 1993). The presence of heavy minerals such as zircon, monazite possibly has considerable effect on the REE pattern of individual samples (Rollinson, 1993). The total REE concentration of the studied samples (ΣREE) is 103.88 ppm, which is lower than the average PAAS (183 ppm) and UCC (145.72 ppm) concentrations (Table-8). The CI-normalized REE patterns are similar to the PAAS and UCC with slightly enriched LREEs, flat HREEs, and a slight negative Eu anomaly (fig-9-B). The Eu anomaly latter was calculated according to (McLennan, 1989):

Where N = chondrite-normalized values.

The Eu anomaly values of greater than 1.0 indicate a positive anomaly while values of less than 1.0 indicate the negative anomaly.

Similar to other LREE, Eu is an incompatible element, however is specially incorporated into plagioclase. Accordingly, the average UCC exhibits Eu depletion through fractionation effects (McLennan, 1989). In all studied samples, the Eu shows a negative anomaly (Eu/Eu*<1) with an average of 0.82, except sample SIT6 (1.03). The mean and median Eu/Eu* is slightly lower than the PAAS and UCC (Table-8). The $(La/Yb)_N$ value, which describes the total slope of the CI-normalized REE trend, is higher than the PAAS (Taylor & McLennan, 1985) in all samples. The chondrite-normalized $(La/Sm)_N$ ratios which indicate the LREE enrichment in this sample ranges from 3.5-4.0 and have an average of 3.7. The $(Gd/Yb)_N$ values range from 1.2-2.1 with average ratios of 1.8 (Table-8)., that indicate flat HREE pattern (fig-9-B).

LOI values for all samples are range from 0.9% (SST3) to 5.15% (MST1). Mudstone sample (MST1) has the highest value of LOI, which is expected in felsic rocks. Sandstone sample (SST3) from Bokotabo-Sentom area has the lowest value of LOI that indicates it is enriched in mafic minerals rather than felsic.

A

B

Figure 9 - (A) The selected major and trace element concentrations normalized to the primitive mantle after (McDonough and Sun, 1989). (B) Rare earth element concentrations, chondrite normalized after (McDonough and Sun, 1995). Patterns for PAAS from (Taylor and McLennan, 1985) and UCC from (McLennan, 2001) have been plotted for comparison.

4.2.1.2. The Daguja area sandstone

The selected major and trace elements normalized to upper continental crust and shale, and chondrite normalized REE are plotted in (fig-11). SiO_2 concentrations in the Daguja area range from 65.3 – 76.5 wt. %. The relative enrichment of Al_2O_3 (12.2 – 13.95 wt. %, mean – 12.97 wt. %), Na_2O (1.96 - 4.81 wt. %, mean 3.7 wt. %), and K_2O (1.01 – 4.1 wt. %, mean – 2.28 wt. %) in this area, is possibly due to elevated levels of feldspar. It is also, relatively, enriched in CaO (0.42 - 5.94 wt. %, mean 2.34 wt. %), Fe_2O_3 (1.27 - 3.09 wt. %, mean 1.91 wt. %), MgO (0.12 - 1.85 wt. %, mean 1.03 wt. %), TiO_2 (0.15 - 0.47 wt. %, mean 0.32 wt. %), P_2O_5 (0.04 - 0.17 wt. %, mean 0.09 wt. %), and MnO (0.02 - 0.11 wt. %, mean 0.05 wt. %) when compared with Bokotabo-Sentom area. The siltstone samples in this area are relatively enriched in CaO. SiO_2/ Al_2O_3 ratio values of the studied samples range from 5.12 to 6.32. All samples show low CaO/ Al_2O_3 values (0.034 to 0.466), but relatively high when compared with Bokotabo-Sentom area sandstones. All samples generally have low concentrations of TiO_2 (<1 wt. %) which indicates low abundances of Ti-bearing opaque minerals such as rutile (Table-4). The studied samples show high contents of SiO_2 and Na_2O and low in Fe_2O_3, Al_2O_3, MgO, and TiO_2 contents, when compared with UCC (Mclennan, 2001) and PAAS (Taylor and McLennan, 1985). Siltstone (sampled as SIT1) has a higher value of CaO (5.94%) and enriched in Fe_2O_3 content. The tillite (TIL1) has a higher value of K_2O (4.1%) than the UCC and PAAS which is mainly controlled by the presence of K-feldspar (K-mica) (Wedepohl, 1978).

The SiO_2 concentration shows a strong negative correlation with Fe_2O_3, MnO, CaO, and P_2O_5, while Al_2O_3 and K_2O exhibit no correlation with SiO_2 (Table-6). Al_2O_3 shows a strong negative correlation with MgO and TiO_2, a strong positive correlation with K_2O, and weak positive correlation with Na_2O, and no correlation with CaO, P_2O_5, Fe_2O_3, and SiO_2 (fig-10). The enrichment of Na_2O (1.96 - 4.81 wt. %, average - 3.7%) in these samples can be attributed to a relatively higher amount of Na-rich plagioclase in them. The K_2O and Na_2O contents and their ratios (K_2O/Na_2O) in all samples are <1. The tillite samples are relatively enriched in Al_2O_3 and K_2O content. All samples have correspondingly increased concentrations of trace elements (Zr, Th, Y, and REEs like La, Ce, Sm, Gd, Tb, and Dy) (Table-5).

All sandstone and siltstone samples have higher LOI values (4.04%-4.95%), which is expected in felsic sediments, while the tillite has lesser value (0.67%).

Figure 10 - Multiple plots of Al_2O_3 against all major elements the Daguja area (A) Al_2O_3 vs SiO_2, (B) Al_2O_3 vs CaO, (C) Al_2O_3 vs MgO, (D) Al_2O_3 vs Na_2O, (E) Al_2O_3 vs K_2O, (F) Al_2O_3 vs TiO_2, (G) Al_2O_3 vs P_2O_5, and (H) Al_2O_3 vs Fe_2O_3; all major elements are measured by (w.%).

Large-ion lithophile elements: Rb, Sr, and Cs concentrations in all samples are well below the UCC values, while all samples enriched in Ba compared to the UCC except sandstone samples (SST1). Rb, Cs, and Ba concentrations relatively enriched in the tillite unit while Sr enriched in siltstone samples. Cs, Rb, and Ba show a strong positive correlation with Al_2O_3 (Table-9).

High field strength elements: Th, U, Y, Hf, Nb, and Ta in all studied samples are well below UCC (fig-11-A). Sandstone sample (SST1) relatively enriched in elements such as Hf, Sm, and Zr, and depleted in Ga, and V (Table-5). Siltstone (SIT1) is relatively enriched in Y, V, Zn, and Ta, while depleted in Th. And the tillite relatively enriched in Ga, and depleted in Zr, Sm, Y. Th shows a strong positive correlation with Al_2O_3 (r=852818) and strong negative correlations with elements, such as TiO_2 and Nb (r =-0.97709 and r=-0.99785, respectively) (table-9).

Transition trace elements: All transition trace elements are depleted in the studied samples as compared to the UCC value. Sample SIT1 is enriched in Sc and Ni while the tillite is enriched in Cu (Table-5). Strong negative correlations between Cu and Ni (r=-0.71543) have been observed. Sc correlates strongly positive with TiO_2 (r= 0. 827788) and correlates weakly with Al_2O_3 (r= -0.20968), Zr (r=-0.13618) and the REEs (r= 0.140108) (Table 7&9).

Rare earth elements: The average total REE concentration (ΣREE) 87.34667 ppm, much lower than the average PAAS and UCC concentrations (Table-8). CI-normalized REE patterns are similar to the PAAS and UCC with enriched LREEs, flat HREEs (fig-11-B). In all Daguja samples, Eu is well above the UCC values, except the tillite unit sample, which indicates Na_2O enrichment (fig-11-B).

The $(La/Yb)_N$ value, which describes the total slope of the CI-normalized REE trend, is higher than the PAAS (Taylor & McLennan, 1985) in all samples. The chondrite-normalized $(La/Sm)_N$ ratios which indicate the LREE enrichment in this sample are range from 2.5-3.1 and have an average of 2.9. The $(Gd/Yb)_N$ values are range from 0.5-2.3 with average ratios of 1.3, which indicate…at HREE pattern (Table-8).

A

B

Figure 11- (A) selected major and trace element concentrations normalized to the primitive mantle after (McDonough and Sun, 1989), (B) Rare earth element concentrations, chondrite normalized after (McDonough and Sun, 1995). Patterns for PAAS from (Taylor and McLennan, 1985) and UCC from (McLennan, 2001) have been plotted for comparison.

Classification of the upper Paleozoic sandstones

The chemical classification of sandstone was proposed by (Lindsey, 1999) based on major elements (Table-1). Though, it is controversial to differentiate arkose and lithicarenite.

Using the geochemical classification diagram of (Pettijohn et al., 1972), the log (SiO_2/Al_2O_3) vs. log (Na_2O/ K_2O), all siltstones and mudstone from Bokotabo-Sentom area and tillite unit form Daguja area are classified as arkosic, while sandstone and siltstone from Daguja area are classified as lithicarenite, and sandstone from Bokotabo-Sentom area is classified as sub-lithicarenite (fig-12). Based on the classification diagram of (Herron, 1988), the log (SiO_2/Al_2O_3) vs. log (Fe_2O_3/K_2O), mudstone and sandstones from Bokotabo-Sentom area fall on Fe-sand field, while sandstone and siltstone from the Daguja area fall on lithicarenite field, and siltstones and tillite unit form Daguja area fall on arkose field

Table 1 Chemical classification of the upper Paleozoic sandstones based on (Lindesy, 1999)

Classes	log (SiO_2/Al_2O_3)	log (K_2O/Na_2O)	log ((Fe_2O_3+MgO)/(K_2O+ Na_2O))
quartzarenite	>= 1.5	_	_
greywacke	> 1	< 0	_
Arkose(sub-arkose)	< 1.5	>= 0	< 0
Lithic-arenite (subgraywack and protoquartzite)	>1.5	< 0	>0

Samples	Log (SiO_2/Al_2O_3)	Log (K_2O/Na_2O)	Log ((Fe_2O_3+MgO)/ (K_2O+Na_2O))	Chemical classification
SIT5(BOK)	0.86	-0.37	0.77	Arkose
SIT6(BOK)	0.84	-0.31	1.50	Arkose/Lithicarenite
SST5(BOK)	1.51	0.60	0.41	Quartzarenite
SST3(BOK)	1.49	-0.14	1.02	Arkose/Lithicarenite
SIT1(DAG)	0.71	-0.44	0.89	Arkose
SST1(DAG)	0.80	-0.29	0.16	Arkose

A

B

Figure 12- Geochemical classification of (A) the log (SiO_2/Al_2O_3) vs. log (Na_2O/ K_2O) (Pettijohn et al., 1972), (B) the log (SiO_2/Al_2O_3) vs. log (Fe_2O_3/K_2O) (Herron, 1988) for upper Paleozoic sandstone, in both Bokotabo- Sentom and Daguja area.

The Al_2O_3/TiO_2 vs. (SiO_2) plot of (Le Bas et al., 1986) was used to determine the sample whether is felsic or mafic in composition (fig-13A). The geochemical differences between elements such as Th and La (felsic igneous sources indicator) and V, Sc, and Cr (mafic igneous sources indicator) are used as an indicator of contrasting felsic and mafic provenance by using ternary plots such as Ni-V-Th*10 plots (fig-13B) (Condie and Wronkiewicz, 1990; McLennan and Taylor, 1991 and Pacciali et al., 2007). Based on both diagrams, the upper Paleozoic sandstone in both sections is felsic in composition. But sandstone from the Daguja area is close to the mafic field because it has a higher amount of V. The granitoid boulders sampled from tillite have similar compositions to those in the granitoid which is underline the tillite.

A

B

Figure 13 „ (A) The Al_2O_3/TiO_2 vs. (SiO_2) relationship to determine whether upper Paleozoic sandstone is felsic or mafic (Le Bas et al., 1986) (B) Ternary Ni, V, Th*10 diagrams for source rock discrimination after (Bracciali et al., 2007)

4.2.2. Paleoclimate condition

4.2.2.1. Major Oxide€s climate proxies

4.2.2.1.1. CIA, CIW , and PIA

Chemical weathering affects the mineralogy of rocks and sediments that leads to affecting their major element composition. The degree of chemical weathering possibly acquired by the chemical index of alteration (CIA), plagioclase index of alteration (PIA), and chemical index of weathering(CIW) on a molecular basis of the major element oxides to evaluating how these processes have affected the rocks and sediments, proposed by (Nesbitt and Young, 1982).

CIA = (") " 100 ƒƒƒƒƒƒ. Equation (1)

PIA = (") " 100 ƒƒƒƒƒƒƒ Equation (2)

CIW = (") " 100 ƒƒ.ƒƒƒƒƒƒƒ Equation (3)

CaO* represents CaO incorporated in silicate minerals and accepted when CaO ≤ Na_2O (Fedo et al., 1995). CaO was low in all measured samples. Therefore, CaO* was considered as equal to CaO. High CIA, PIA, and CIW values (75–100) shows intensive weathering history in the source area, while low values (60 or less) indicate low weathering in the source area. The CIA CIW and PIA were calculated and presented in (Table 4).

Bokotabo-Sentom area

The calculated CIA values for studied Bokotabo-Sentom samples range from 63.4 (sample SIT6) to 94.5 (sample MST1), with an average of 73.9. The PIA values range from 52.1 (sample SIT6) to 89.7 (sample MST1), with an average of 64.8. The CIW values range from 71.5 (sample SIT6) to 99.4 (sample MST1) with an average of 81.0. The mudstone sample (MST1) has relatively the highest value of CIA, PIA, and CIW that shows the highest chemical weathering history. While the siltstone sample SIT6 has the lowest value that indicates the lowest weathering history

Daguja area

The CIA values for these samples are range from 60.5 (for tillite unit) to 78.3 (sample SST1), with an average value of 68.3. The PIA values range from 42.8 (for tillite unit) to 71.8 (sample SST1), with an average of 57.2. The CIW values range from 54.3 (sample SIT1) to 83.7 (sample SST1) with an average of 70.5. The tillite sample (TIL1) has the lowest value of CIA and PIA and CIW while the sandstone sample (SST1) has the highest value of CIA, CIW, and PIA.

4.2.2.1.2. The A CN K diagram

Paleo-weathering conditions can also be identified using the Al_2O_3 - (CaO*+Na_2O) - K_2O (A-CN-K) ternary diagram of Nesbitt and Young (1984), where unweathered rocks are crowded together alongside the K-feldspar-plagioclase join (Nesbitt and Young, 1984; Holail and Moghazi, 1998). All the studied samples examined here in both area plot parallel to the A-CN line (Fig-14). The Bokotalo-Sentom sections show medium to high weathering conditions, while the Daguja section shows low to medium weathering conditions.

A bivariate plot of SiO_2 against total Al_2O_3+K_2O+NaO as proposed by Suttner and Dutta (1986) was used to classify the maturity of sandstones (Zaid and Al Gahtani, 2015), and all samples in both areas lie on semi-arid fields, except sandstone (SST3) which lies on semi-humid fields (fig-15).

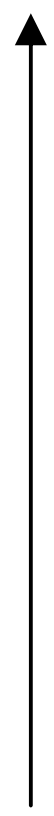

Figure 14 - A„ CN„ K ternary diagram [Al_2O_3 - (CaO^*+Na_2O) „ K_2O] ; for both study areas, Bokotabo-Sentom area Daguja area after (Nesbitt and Young, 1984).

Figure 15 Chemical maturity of the upper Paleozoic sandstones stated by bivariate plots of SiO_2 vs $Al_2O_3+K_2O+Na_2O$ after (Suttner and Dutta, 1986)

4.2.3 Tectonic setting

Based on the Petrographic approach, Dickinson and Suczek (1979), and Dickinson et al. (1983) worked on the relationship between sandstone compositions and tectonic setting. Dickinson and Suczek (1979) proposed that tectonic settings of depositional basins are recognized by plotting the detrital framework modes of sandstone suites on QFL and QmFLt ternary diagrams (Dickinson and Suczek, 1979; Dickinson et al., 1983). The QFL (Quartz-Feldspar-Lithics) diagram is grouped into three main fields that are representative of three different tectonic regimes, named: "continental blocks," "magmatic arcs," and "recycled orogen" (Dickinson et al., 1983), and plotted on (fig-19-A). The QmFLt diagram is comparable to the QFL diagram, except that it plots exclusively monocrystalline quartz (Qm), and total lithics (Lt) (Dickinson et al., 1983) and plotted on (fig-19-B).

For selected major elements, trace elements and REEs, valuable comparison can be made with sandstones derived from known tectonic settings. Various authors have depicted that the effectiveness of major element geochemistry of sedimentary rocks to identify tectonic settings based on discrimination diagrams (Bhatia, 1983; Roser and Korsch, 1986). Armstrong-Altrin and Verma (2013) proposed two new discrimination function-based diagrams for siliciclastic sediments from 3 main tectonic settings; continental rift, arc, and collision. These diagrams were used to distinguish the tectonic setting of siliciclastic sediments by employing major elements and optimized for both low silica (35% to 63% SiO_2) and high silica rocks (63% to 95% SiO_2). They are tested on Neogene-Quaternary as well as Precambrian sediments with success rates of 75% to 100% (Verma and Armstrong, 2013; Bassis, 2017). In these diagrams, three different tectonic settings were considered: (1) "Arc" field (Continental and ocean island arcs), (2) "Collision" field (continental collision), and (3) "Rift" field (continental rifting leading to the development of passive margins and intra-cratonic basins) (Verma and Armstrong, 2013). The equations for the Discrimination functions (DF1 and DF2) were programmed for the high-silica ([(SiO_2) = > 63 % to <=95 %] sediments) and low-silica (SiO_2)adj =>35%- <=63 %) sediments (Verma and Armstrong, 2013). It excludes all samples with (SiO_2)adj>95% and (SiO_2) <35% as suggested by the original authors (Verma and Armstrong, 2013). Since the silica content in the upper Paleozoic sandstones is >= 65, high-silica sediment equations were used for this thesis. Samples with (SiO_2)adj> 95 % are excluded, for the reason that they possibly characterize relatively high analytical errors in the determination of the major elements (Verma and Armstrong, 2013).

$$DF1_{(Arc\text{-}Rift\text{-}Col)\,ml} = (-0.263 * \ln(TiO_2/SiO_2)_{adj}) + (0.604*\ln(Al_2O_3/SiO_2)_{adj}) + (-1.725*\ln(Fe_2O^t_3/SiO_2)_{adj}) + (0.660*\ln(MnO/SiO_2)_{adj}) + (2.191*\ln(MgO/SiO_2)_{adj}) + (0.144*\ln(CaO/SiO_2)_{adj}) + (-1.304*\ln(Na_2O/SiO_2)_{adj}) + (0.054*\ln(K_2O/SiO_2)_{adj}) + (-0.330*\ln(P_2O_5/SiO_2)_{adj}) + 1.588$$

$$DF2_{(Arc\text{-}Rift\text{-}Col)\,ml} = (-1.196 * \ln(TiO_2/SiO_2)_{adj}) + (1.064*(\ln Al_2O_3/SiO_2)_{adj}) + (0.303*\ln(Fe_2O^t_3/SiO_2)_{adj}) + (0.436*(\ln MnO/SiO_2)_{adj}) + (0.838*\ln(MgO/SiO_2)_{adj}) + (-0.407*(\ln CaO/SiO_2)_{adj}) + (1.021*\ln(Na_2O/SiO_2)_{adj}) + (-1.706*(\ln K_2O/SiO_2)_{adj}) + (-0.126*\ln(P_2O_5/SiO_2)_{adj}) - 1.068$$

The subscript adj in $(SiO_2)_{adj}$ refers to the SiO_2 value obtained after volatile-free adjustment of the ten major-elements to 100 wt.%.

The tectonic setting discrimination diagram of Verma and Armstrong-Altrin (2013) based on major oxide concentrations are plotted on (fig-16). All samples from the Daguja area and SIT5 from the Bokotabo-Sentom area plotted in the €continental rift• and all samples from the Bokotabo-Sentom area, except SIT5, plotted in the €arc• field. In the tectonic discrimination diagram of (Roser and Korsch, 1986) based on major oxides, all sample except mudstone, are allocated to an active margin setting (fig-17). A passive margin setting is distinct by silica-rich sands (SiO_2=70%) with (K_2O/ Na_2O) ratio of more than unity (Bhatia, 1983) and FeO + MgO content of less than 5% (Taylor and McLennan, 1985). Depend on these; mudstone from the Sentom area is correlated with passive margin setting.

Figure 16 Tectonic discriminant function diagrams for the upper Paleozoic Sandstone proposed by (Verma and Armstrong, 2013).

Figure 17 Tectonic setting discrimination diagrams based on major oxides, ARC- Oceanic island arc, AM- active continental margin, PM- passive margin, after (Roser and Korsch, 1986).

5. DISCUSSION

5.1. Implications for provenance

The most relevant features that are used to interpret the provenance of sandstone are the chemical composition of the rocks, which helps to interpret source rock lithology and the direct observation of features (sedimentary structures and grain size and shape) in the rocks (Boggs, 2009).

Sandstones with less abundant quartz and enriched in unstable minerals (lithics, feldspar) have resulted from short transport distances that will allow less stable materials (such as lithic fragments) to survive and get deposited (Dickinson et al., 1983; Johnsson, 1993). Straight to slightly undulate extinction of monocrystalline quartz grains in the sampled thin sections point towards the granitic source (Pettijohn et al., 1987). Inclusions of heavy minerals like zircon and tourmaline in monocrystalline quartz in the studied samples direct evidence of the granitic source. However, some monocrystalline quartz is excluded from these heavy mineral inclusions and shows slight undulate extinction indicates that the source might be older gneiss or schist rocks (Pettijohn, 1975). Polycrystalline quartz with stretched grains and sutured boundaries are derivate from metamorphic source, apparently schistose (Blatt, 1967; Folk, 1980). Therefore, the whole quartz analysis in the studied samples points toward granitic and schistose provenance.

Feldspar is more significant to offer information about primary source rocks composition than quartz because they are chemically and mechanically less stable and less likely to be recycled (Boggs, 2009). A high abundance of feldspars in the sampled thin sections proposed the origin from crystalline rocks (Folk, 1980). Microcline, in the studied samples, indicates the origin of felsic igneous or metamorphic rocks (Boggs, 2009). According to Pittman (1963), unzoned plagioclase is to be likely from a metamorphic origin (Krainer & Spotl, 1989). Unzoned plagioclase in the sampled thin sections probably is sourced from low-grade metamorphic rocks, such as slate. The presence of micro-perthitic intergrowths in the sampled thin sections suggests it sourced from an igneous rock, granites (Folk 1980). The presence of zircon and rutile in the sampled thin section indicates an acid igneous source (Pettijohn, et al., 1987). Based on feldspar in the studied samples, the upper Paleozoic sandstone is feldspar rich arkosic lithology which indicates that local deposits derived from low to medium grade metamorphic rocks (slate and schistose) and granitic basement rocks (Pettijohn et al., 1972; Miall, 1984). Based on feldspar content, the upper Paleozoic sandstone is compositionally immature (in the Daguja area) to sub-mature (in the Bokotabo-Sentom area).

Rock fragments are also giving the best clue to the provenance of rocks. The presence of siltstone and sandstone rock fragments in the sampled thin section indicates sedimentary origin, while, plutonic lithic fragment include clasts of quartz and feldspar are granitoid in origin.

Clay minerals are excellent for provenance studies because individual clay minerals are typically formed by the weathering of particular bedrock types (Blatt, 1985; Nichols, 2009). The presence of mica (muscovite and biotite), in the sampled thin section, probably indicates low-grade metamorphic rocks origins like schist, gneiss and granite (Ghazi, 2009).

According to the QFL triangular diagram (McBride, 1963), the classification of the upper Paleozoic sandstones is arkosic.

Figure 18 The QFL triangular diagram shows the classification of the upper Paleozoic sandstones, after (McBride, 1963).

The SiO_2 contents and SiO_2/Al_2O_3 ratio and the alkali content ($Na_2O + K_2O$) are the most used geochemical criteria for sedimentary maturity. They are reflecting the quantity of silica (quartz), clay, and feldspar contents (Potter, 1978 and Rollinson, 1993). The negative correlation between SiO_2 and Al_2O_3, indicating that much of the SiO_2 is present as quartz grains (Akarish and El-Gohary, 2008; Ahmad and Chandra, 2013). Al enrichment signifies the abundance of feldspar and clay minerals which is related to lower maturity. A positive correlation of Al_2O_3 with K_2O and Na_2O indicates that Al distribution considerably influenced by the concentrations of the feldspars and suggests that the abundance of these elements is mostly controlled by plagioclase and Feldspar-bearing minerals such as clay mineral (mica and muscovite) concentrations (McLennan et al., 1983; Akarish and El-Gohary, 2008). Al_2O_3 and K_2O concentration in the studied samples possibly associated with the presence of K-feldspars (orthoclase and microcline), and mica. The relative enrichment of Na_2O over K_2O in all samples can be attributed to a relatively higher amount of Na-rich plagioclase in them, while depleted in mudstone due to a relatively small amount of Na-rich plagioclase. The K_2O and Na_2O ratios (K_2O/Na_2O) in all samples (except mudstone) are <1% that perhaps according to plagioclase feldspar dominates over K-feldspar. Some samples (typically, siltstone in the Daguja area) are relatively enriched in CaO which possibly due to the presence of diagenetic calcite cement. Some samples (typically, mudstone and siltstone) are enriched in Fe_2O_3 content that is possibly related to the abundance of Fe-oxide heavy minerals. The geochemical classification diagram proposed by (Herron 1988) and (Pettijohn et al., 1972) shows that the upper Paleozoic sandstones are arkosic and Lithicarenite. Based on the A-CN-K ternary diagram, all Formation in both areas was derived from plagioclase-granitic-smectite source terrain. The Al_2O_3/TiO_2 vs. (SiO_2) ratios proposed by (Le Bas et al., 1986) and Ternary Ni, V, Th*10 diagrams (Bracciali et al., 2007) implies the whole the upper Paleozoic sandstone is felsic in composition.

The tillite unit is enriched in Al that signifies the abundances of feldspar and clay minerals which is related to lower maturity. It has a slightly higher amount of Na_2O than the K_2O indicates controlled by the presence of plagioclase than K-feldspar (K-mica) (Wedepohl, 1978)

The most important elements for provenance indicator are REE, Sc, Th, and lesser Cr, Co. These elements are unaffected by diagenesis and metamorphism due to their low concentration in sea and river, and low residence time in the ocean and element ratios. Accordingly, they reflect their source rock chemistry (Rollinson, 1993). Immobile elements such as Zr, Hf, and Sc are possibly controlled by the distribution of heavy minerals and dispersed according to grain size. Co, Cr, Fe, Sc, and Ta that controlled by ferromagnesian minerals are low concentrations in the studied samples (Culler, 1988). Most formations (on average, mudstone in Sentom and sandstones in the Daguja area) have correspondingly increased concentrations of trace elements (Zr, Th, Y, and REEs like La, Ce, Sm, Gd, and Dy), which are indicative of heavy minerals like zircon.

The concentrations of Ba, Rb, and Cs are controlled by feldspar. The enrichment of Ba and Rb in mudstone and siltstone is strongly influenced by the presence of K-feldspar, and mica (biotite and muscovite). Strong positive correlations of Cs, Rb, Sr, and Ba with Al_2O_3 in the studied samples show phyllosilicate (clay minerals and micas) as a controlling factor of LILE concentrations (Etemad-Saeed et al., 2011). The enrichment of LILEs in the upper Paleozoic sandstones is possibly as a result of less weathering and metamorphic processes and controlled by K- feldspar, and mica. As high field strength elements are incompatible and immobile elements, they are a good indicator of provenance (Taylor and McLennan, 1985). Y, Pb, Ti, and Zr enriched in most sandstones and mudstones that indicates felsic source rather than mafic rocks. Th shows strong positive correlations with elements, such as TiO_2 and Nb, which indicates that it is possibly controlled by clays or Ti- and Nb bearing phases associated with clay minerals. Sc correlates strongly positive with TiO_2, this may indicate heavy minerals as controlling factors for Sc concentrations (Etemad-Saeed et al., 2011). The depletion of Sc, V, Co, Ni, and Cr in most samples is due to the depletion of mafic minerals in them, low concentration of these elements in the studied samples is related to felsic provenance rather than mafic composition. Although rare earth elements are the least concentrated, they are an excellent indicator of provenance due to their immobility during weathering (McLennan, 1989; Rollinson, 1993). Chondrite normalized patterns show moderate LREE enrichment and flat HREE segments. LREE enrichment indicates the sources of felsic crust. Eu which is mostly incorporated in plagioclase is relatively enriched in siltstones in both areas.

5.2. Implications for paleoclimate

Climate is one of the factors that has an intense impact on the composition and maturity of siliciclastic sediments and the climatic signatures are well preserved in the deposited sediments (Suttner and Dutta, 1986).

Based on Petrographic evidence, paleoclimate conditions of the upper Paleozoic sandstone can be determined. For instance, less abundance of rounded quartz, coarse-grained feldspars, and sub-angular grain sizes are related to a low to moderate degree of chemical weathering. Besides, angularities of quartz grains and detrital components, textural immaturity indicate the first cycle of erosion sediments or short distance of transportation before deposition. The sediments which have a high amount of feldspar are immature (Osae et al., 2006). The high proportion of feldspar and the dominance of chemically unstable plagioclase over K-feldspar in the upper Paleozoic sandstones suggest that the source was exposed to low to moderate weathering history. An abundance of unaltered feldspars and lithics in these sandstones suggested that it is sourced from moderate to high relief and rapid erosion and deposition in nearby basins with their insignificant alteration. Color also can give helpful information on lithology, depositional environment. For instance, ferric irons frequently occur as the mineral hematite and provide a red color to the rock. Hematite formed under oxidizing conditions and these are often found within sediments originated under semi-arid environments. Mudrocks formed under these environments (e.g., deserts, lakes, and rivers) are repeatedly reddened through hematite pigmentation. The dominance of unstable grains (feldspar and other rock fragments), the relatively low percentage of monocrystalline quartz (especially in the Daguja area), and the less alteration of feldspar grains implied that the source area experienced a short to moderate period of chemical weathering (Pettijohn et al., 1987; Amireh, 1991).

The degree of chemical weathering can be achieved by calculation of the chemical index of alteration (CIA), plagioclase index of alteration (PIA), and chemical index of weathering (CIW) (Nesbitt and Young, 1982). These CIA and PIA values indicate moderate degrees of weathering of the source, or during transport before deposition, which may reflect first-stage recycling in semi-arid and semi-humid climate conditions in the source area (McLennan et al., 1993; Osea et al., 2006; Bakkiaraj et al., 2010). The studied samples (MST1 in Sentom and SST1 in the Daguja area) have the highest value of CIA, CIW, and PIA which may indicate higher weathering history. The highest values of chemical proxies in the mudstone are due to high chemical weathering such as oxidizing. The rest studied samples' values indicate low to moderate degrees of weathering of the source. Generally, chemical weathering values of the upper Paleozoic sandstone shows moderate to high weathering history in the Bokotabo-Sentom area, and low to moderate degrees of weathering in the Daguja area, that reflect moderate recycling in semi-arid and semi-humid climate conditions in the source area or during transport (McLennan et al., 1993; Osea et al., 2006).

A„ CN„ K ternary diagram of molecular proportions of Al_2O_3 - (CaO*+Na_2O) „ K_2O proposed by after (Nesbitt and Young, 1984), to determine the paleo-weathering of the upper Paleozoic sandstone falls between plagioclase-granite - smectite fields. A-CN-K- diagram shows low-medium to high chemical weathering conditions in both areas. A bivariate plot of SiO_2 against total Al_2O_3+K_2O+Na_2O as proposed by (Suttner and Dutta., 1986) was used to identify the maturity of the upper Paleozoic sandstone as a role of climate. This plot shows that the upper Paleozoic sandstones fall in the semi-arid climatic conditions except for sandstone from the Bokotabo-Sentom area which falls on a semi-humid field.

The tillite unit has the lowest value of CIA and PIA that indicates low weathering history, or direct input of immature continent detrital minerals into the depositional system (Bakkiaraj et al., 2010).

5.3. Implications for tectonic setting

A variety of ternary diagrams (Dickinson and Suczek, 1979; Ingersoll and Suczek, 1979; Dickinson, 1985) were applied to construct the relationship between detrital mineralogy and tectonic setting. Sandstone compositions are related to major provenance types such as stable cratons, basement uplifts, magmatic arcs, and recycled orogens (Dickinson et al., 1983). Sandstones enriched in lithics and less abundant in quartz resulted from short transport distances that decrease physical sediment sorting and chemical weathering and characterized by magmatic arc depositional systems (Dickinson et al., 1983; Johnsson, 1993).

The upper Paleozoic sandstone was plotted on the QFL and QmFLt ternary diagrams of (Dickinson et al., 1983) to interpret the tectonic discrimination source fields (fig-19). In the QFL plot (Dickinson, 1985) the selected samples are plotted in transitional continental region of continental block provenance fields. This indicates the detritus derived from transitional areas between craton interiors and basement uplift masses. The detritus sediments derived from this field have intermediate compositions between craton (pure quartzose sand) and uplifted basement (arkosic sands). In the QmFLt plot (Dickinson, 1985) most of the samples from the Daguja area, fall in basement uplift fields while most of the samples that are from Bokotabo-Sentom area plotted in the transitional continental region.

Figure 19 The QFL and QmFLt ternary diagram for tectonic discrimination of the upper Paleozoic sandstone after (Dickinson et al., 1985).

Different tectonic environments do have a distinctive geochemical signature, therefore, geochemical data can be used to extract important environmental information from such source that assign tectonic environments (Mclennal et al., 1990; Rollinson, 1993). Fe, Mg, Ti, and Al are more abundant in Arc-derived sediments rather than cratonic and recycled sediments. Most of the studied samples from both areas are enriched in Al and Fe. Sediments derived from transitional recycled sources are moderately enriched in the light rare earth elements (REE) and flat HREE slopes, without the pronounced flattening seen in other cratonic sediments. All studied samples from both areas show moderately enriched in the light rare earth elements (REE) and flat HREE slopes.

The discriminant function diagram which is used to evaluate the tectonic setting for the upper Paleozoic sandstones suggests that the upper Paleozoic sandstone possibly derived from the continental arc and continental rift. Based on major oxides, on active versus passive margin diagram of (Roser and Korsch, 1986), all samples, except mudstone are derived from active margin setting. Mudstone is derived from a passive margin setting.

Comparision of the upper Paleozoic sandstone in Blue Nile Basin and Mekele Basin

The upper Paleozoic sandstones in the Blue Nile Basin consist of tillite sandstone and siltstone, around the Daguja area and sandstone, siltstone, and mudstone around the Bokotabo-Sentom area. In Mekelle basin, it consists of tillite at the base overlain by laminated clay and siltstones (Edaga Arbi Glacials) and basal tillite, a lower glaciogenic sandstone unit and an upper shallow marine sandstone unit (Enticho Sandstone) (Lewin et al., 2018).

The upper Paleozoic sandstone in Blue Nile Basin and Edaga Arbi Glacials in Mekele Basin has similarity in source composition and provenance, based on petrographic and geochemical results. Both show juvenile, crustal sources such as the Arabian-Nubian Shield. The upper Paleozoic sandstones in the Blue Nile Basin are arkose and lithicarenite, while sub-arkose to arkose in the Mekele Basin. Accessory minerals such as zircon, tourmaline, rutile, garnet, and opaque minerals are observed in both formation. Both formations show Al, Na, and K enrichment that indicates a low maturity of the rock. However, there is a slight difference between their CIA values which indicates paleo-weathering and tectonic setting discrimination. Based on CIA value, the upper Paleozoic sandstones in the Blue Nile Basin show low to medium-high weathering history while the Mekele Basin has low weathering history. In the tectonic setting discrimination diagram of Verma and Armstrong-Altrin (2013) based on major oxide concentrations, the upper Paleozoic sandstones in the Blue Nile Basin shows "continental rift" and "arc," while in the Mekele Basin it shows "continental rift" and "collision" fields. In the active versus passive margin discrimination, the upper Paleozoic sandstones in the Blue Nile Basin are assigned in the passive margin setting while the Mekele Basin are assigned in the active and passive margin setting.

6. CONCLUSIONS AND RECOMMENDATION

Based on the petrological and geochemical analysis of the upper Paleozoic sandstones (Permo-Carboniferous), the following conclusions can be drawn:

- The upper Paleozoic sandstone has a provenance transitional continental and basement uplift with a mixture of acid igneous, meta-sedimentary, and low-grade metamorphic rocks. It is compositionally immature to sub-mature and has been classified as arkosic and lithic arenite in composition. Additionally, some euhedral heavy minerals (zircon and tourmaline grains) show short transport distances. Therefore, it was derived from the basement rocks nearby, possibly Neo-Proterozoic granitoid rocks and low-grade metamorphic rock (slate and schist). Based on the above statement and trace element geochemistry, the Neoproterozoic basement of the nearby ANS is almost certainly the source.
- The upper Paleozoic sandstone has moderate to high weathering history in the Bokotabo-Sentom area, and low to moderate weathering history in the Daguja area. Paleoclimate data for the upper Paleozoic sandstone suggests semi-arid climate conditions for all sandstones in both areas and semi-humid climate conditions for sandstone from the Bokotabo-Sentom area.
- The tectonic setting discriminant diagram suggests that deposition of the sediments is in the continental arc and continental rift fields. Based on the active and passive diagram, all sediments are derived from the active margin, and mudstone is derived from the passive margin.

Recommendation

Isotopic analysis (that reduces the influence of sedimentary sorting on provenance studies) are required to have a better understanding of the provenance, tectonic setting, and paleo-weathering history.

References

Abbate, E., Bruni, P., & Sagri, M. (2015). Geology of Ethiopia: a review and geomorphological perspectives. In Landscapes and landforms of Ethiopia (pp. 33-64). Springer, Dordrecht.

Ahmad, I., & Chandra, R. (2013). Geochemistry of loess-paleosol sediments of Kashmir Valley, India: provenance and weathering. Journal of Asian Earth Sciences, 66, 73-89.

Akarish AIM, El-Gohary AM (2008). Petrography and geochemistry of lower Paleozoic sandstones, East Sinai, Egypt: implications for provenance and tectonic setting. J Afr Earth Sci 52: 43-54.

Aleali, M., Rahimpour-Bonab, H., Moussavi-Harami, R., & Jahani, D. (2013). Environmental and sequence stratigraphic implications of anhydrite textures: A case from the Lower Triassic of the Central Persian Gulf. Journal of Asian Earth Sciences, 75, 110-125.

Amireh, B. S. (1991). Mineral composition of the Cambrian-Cretaceous Nubian series of Jordan: provenance, tectonic setting and climatological implications. Sedimentary Geology, 71(1-2), 99-119.

Armstrong Altrin JS, Verma SP (2005). Critical evaluation of six tectonic setting discrimination diagrams using geochemical data of Neogene sediments from known tectonic setting. Sediment Geol 177: 115-129.

Assefa, G. (1981). Gohatsion formation: a new Liasmal lithostratigraphic unit from the Abby River basin, Ethiopia. Geoscience Journal, 2, 63-88.

Assefa, G. (1991). Lithostratigraphy and environment of deposition of the Late Jurassic-Early Cretaceous sequence of the central part of Northwestern Plateau, Ethiopia. Neues Jahrbuch für Geologie und Paläontologie-Abhandlungen, 255-284.

Bakkiaraj R, Nagendra, Nagarajan R, Armstrong-Altrin JS (2010). Geochemistry of sandstones from the Upper Cretaceous Sillakkudi Formation, Cauvery basin, southern India: implication for provenance. J Geol Soc India 76: 453-467.

Bas, M. L., Maitre, R. L., Streckeisen, A., Zanettin, B., & IUGS Subcommission on the Systematics of Igneous Rocks (1986). A chemical classification of volcanic rocks based on the total alkali-silica diagram. Journal of petrology, 27(3), 745-750.

Bassis, A. (2017). Petrography, geochemistry, and provenance of Saudi Arabian Palaeozoic sandstones (Doctoral dissertation, Technische Universität).

Bauluz, B., Mayayo, M. J., Fernandez-Nieto, C., & Lopez, J. M. G. (2000). Geochemistry of Precambrian and Paleozoic siliciclastic rocks from the Iberian Range (NE Spain): implications for source-area weathering, sorting, provenance, and tectonic setting. Chemical Geology, 168(1-2), 135-150.

Bhatia, M. R. (1983). Plate tectonics and geochemical composition of sandstones. The Journal of Geology, 91(6), 611-627.

Bhatia, M. R., & Crook, K. A. (1986). Trace element characteristics of graywackes and tectonic setting discrimination of sedimentary basins. Contributions to mineralogy and petrology, 92(2), 181-193.

Billi, P. (Ed.). (2015). Landscapes and landforms of Ethiopia. Springer.

Blatt, H. (1967). Provenance determinations and recycling of sediments. Journal of Sedimentary Research, 37(4), 1031-1044.

Blatt, H. (1985). Provenance studies and mudrocks. Journal of Sedimentary Research, 55(1), 69-75.

Boggs Jr, S., & Boggs, S. (2009). Petrology of sedimentary rocks. Cambridge university press.

Bracciali L, Marroni M, Pandolfi L, Rocchi S (2007) Geochemistry and petrography of western Tethys Cretaceous sedimentary covers (Corsica and the northern Apennines): from source areas to configuration of margins. In: Arribas J, Critelli S, Johnsson MJ (eds), Sedimentary provenance and petrogenesis: perspectives from petrography and geochemistry, vol. 420, Geol Soc Am Spec Pap, pp 73-93

Bussert, R. (2010). Exhumed erosional landforms of the Late Palaeozoic glaciation in northern Ethiopia: indicators of ice-flow direction, palaeolandscape and regional ice dynamics. Gondwana Research 18, 356-369.

Bussert, R. & Schrank, E. (2007). Palynological evidence for the latest Carboniferous-Early Permian glaciation in Northern Ethiopia. J. Afr. Earth Sci. 49: 201-210.

Collins, A. S., & Pisarevsky, S. A. (2005). Amalgamating eastern Gondwana: the evolution of the Circum-Indian Orogens. Earth-Science Reviews, 71(3-4), 229-270.

Condie, K. C., & Wronkiewicz, D. J. (1990). The Cr/Th ratio in Precambrian pelites from the Kaapvaal Craton as an index of craton evolution. Earth and Planetary Science Letters, 97(3-4), 256-267.

Cullers, R. L., Basu, A., & Suttner, L. J. (1988). Geochemical signature of provenance in sand size material in soils and stream sediments near the Tobacco Root batholith, Montana, USA. Chemical Geology, 70(4), 335-348.

Dawit, E.L., (2014). Permian and Triassic micro-floral assemblages from the Blue Nile Basin, central Ethiopia. Journal of African Earth Sciences 99, 408-426.

Dawit, E., & Bussert, R. (2009). Stratigraphy and facies architecture of Adigrat Sandstone, Blue Nile Basin, Central Ethiopia. Zentral Blatt Geol Paläontol, 1, 217-232.

Dickinson WR (1970) Interpreting detrital modes of greywacke and arkose. J Sediment Petrol 40: 695• 707.

Dickinson, W. R. (1985). Interpreting provenance relations from detrital modes of sandstones. In Provenance of arenites (pp. 333-361). Springer, Dordrecht.

Dickinson, W. R., & Suczek, C. A. (1979). Plate tectonics and sandstone compositions. Aapg Bulletin, 63(12), 2164-2182.

Dickinson, W. R., Beard, L. S., Brakenridge, G. R., Erjavec, J. L., Ferguson, R. C., Inman, K. F., ... & Ryberg, P. T. (1983). The provenance of North American Phanerozoic sandstones in relation to tectonic setting. Geological Society of America Bulletin, 94(2), 222-235.

Elhebiry, M. S., Sultan, M., & Kehew, A. (2019). Late Ordovician ice stream in NE Africa and Arabia and its implication. AGUFM, 2019, C21E-1492.

Enkurie, D. L. (2010). Adigrat sandstone in Northern and Central Ethiopia: stratigraphy, facies, depositional environments, and palynology.

Etemad-Saeed, N., Hosseini-Barzi, M., Armstrong-Altrin, J.S. (2011). Petrography and geochemistry of clastic sedimentary rocks as evidence for the provenance of the Lower Cambrian Lalun Formation, Posht-e-badam block, Central Iran. Journal of African Earth Sciences 61, 142-159.

Fedo, C. M., Wayne Nesbitt, H., & Young, G. M. (1995). Unraveling the effects of potassium metasomatism in sedimentary rocks and paleosols, with implications for paleo-weathering conditions and provenance. Geology, 23(10), 921-924.

Folk, R. L. (1974). Petrology of sedimentary rocks: Austin. Texas, Hemphill, 182.

Folk, R. L. (1980). Petrology of sedimentary rocks. Hemphill publishing company.

Gani, N. D., Abdelsalam, M. G., Gera, S., & Gani, M. R. (2009). Stratigraphic and structural evolution of the Blue Nile Basin, northwestern Ethiopian plateau. *Geological Journal*, 44(1), 30–56.

Gazzi P (1966). Le arenarie del flysch sopracretaceo dell' Appennino modensese: correlazioni con il flysch di Monghidoro. Mineralogica et Petrographica Acta 12: 69–97.

Geletu, S. & Wille, W. (1998). Middle Triassic palynomorphs from the Fincha river valley section, Horo Guduru, western central Ethiopia. N. JB. Geol. Paläont. Mh 5: 257–268.

Ghazi, S. (2009). Sedimentology and stratigraphic evolution of the Early Permian Warchha Sandstone, Salt Range, Pakistan (Doctoral dissertation, University of Leeds).

Herron MM (1988). Geochemical classification of terrigenous sands and shales from core or log data. J Sediment Petrol 58: 820–829.

Holail HM, Moghazi AM (1998). Provenance, tectonic setting, and geochemistry of greywackes and siltstones of the Late Precambrian Hammamat Group, Egypt. Sediment Geol 116: 227–250.

Ingersoll, R. V., & Suczek, C. A. (1979). Petrology and provenance of Neogene sand from Nicobar and Bengal fans, DSDP sites 211 and 218. *Journal of Sedimentary Research*, 49(4), 1217–1228.

Ingersoll RV, Bulard TF, Ford RL, Grimn JP, Pickle JP, Sares SW (1984). The effect of grain size on detrital modes: a text of the Gazzi-Dickinson Point Counting method. J Sediment Petrol 54: 103–116.

Isbell, J.L., Henry, L.C., Gulbranson, E.L., Limarino, C.O., Fraiser, M.L., Koch, J., Ciccioli, P.L., Dineen, A.A. (2012). Glacial paradoxes during the late Paleozoic ice age: evaluating the equilibrium line altitude as a control on glaciation. Gondwana Research 22, 1–19.

Janoušek, V., Farrow, C. M., & Erban, V. (2006). Interpretation of whole-rock geochemical data in igneous geochemistry: introducing Geochemical Data Toolkit (GCDkit). *Journal of Petrology*, 47(6), 1255–1259.

Johnsson, M.J. (1993). The system controlling the composition of clastic sediments. In: Johnsson, M.J., Basu, A. (Eds.), Processes Controlling the Composition of Clastic Sediments, Geological Society of America Special Papers 284, 1–20.

Kazmin, V. (1972). Geology of Ethiopia (explanatory note to the geological map of Ethiopia 1: 2000, 000). The report, Ministry of Mines, Geological Survey of Ethiopia, Addis Ababa, Ethiopia.

Krainer, K., & Spötl, C. (1989). Detrital and authigenic feldspars in Permian and early Triassic sandstones, Eastern Alps (Austria). Sedimentary Geology, 62(1), 59-77.

Le Lewin, A., Meinhold, G., Hinderer, M., Dawit, E.L. & Bussert, R. (2018). The provenance of sandstones in Ethiopia during Late Ordovician and Carboniferous, Permian Gondwana glaciations: Petrography and geochemistry of the Enticho Sandstone and the Edaga Arbi Glacials. Sedimentary Geology, 375, 188• 202.

Lindsey, D. A. (1999). An evaluation of alternative chemical classifications of sandstones (No. 99-346). US Geological Survey.

McBride, E.F. (1963). Classification of common sandstones. Journal of Sedimentary Petrology 33(3), 664• 669.

McDonough, W. F., & Sun, S. S. (1995). The composition of the Earth. Chemical Geology, 120(3-4), 223-253.

McLennan, S.M. (1989). Rare earth elements in sedimentary rocks: influence of provenance and sedimentary processes. In: Lipin, B.R., McKay, G.A. (Eds.), Geochemistry and Mineralogy of Rare Earth Elements. Reviews in Mineralogy 21, 169• 200.

McLennan, S.M. (2001). Relationships between the trace element composition of sedimentary rocks and upper continental crust. Geochemistry, Geophysics, Geosystems 2(4). doi:10.1029/2000GC000109.

McLennan, S. M., & Taylor, S. R. (1991). Sedimentary rocks and crustal evolution: tectonic setting and secular trends. The Journal of Geology, 99(1), 1-21.

McLennan, S. M., Taylor, S. R., & Eriksson, K. A. (1983). Geochemistry of Archean shales from the Pilbara Supergroup, Western Australia. Geochimica et Cosmochimica Acta, 47(7), 1211-1222.

McLennan SM, Taylor SR, McCulloch MT, Maynard JB (1990). Geochemical and Nd-Sr isotopic composition of deep-sea turbidites: crustal evolution and plate tectonic associations. Geochim Cosmochim Ac 54: 2015• 2050.

McLennan, S.M., Hemming, S., McDaniel, D.K., Hanson, G.N. (1993). Geochemical approaches to sedimentation, provenance, and tectonics. In: Johnsson, M.J., Basu, A. (Eds.), Processes Controlling the Composition of Clastic Sediments, Geological Society of America Special Papers 285, 21–40.

Miall, A. D. (1984). Sedimentation and tectonics of a diffuse plate boundary: the Canadian Arctic Islands from 80 Ma BP to the present. Tectonophysics, 107(3-4), 261-277.

Mogessie, A., Krenn, K., Schaflechner, J., Koch, U., Egger, T., Goritchnig, B., ...& Tadesse, S. (2002). A geological excursion to the Mesozoic sediments of the Abay Basin (Blue Nile), recent volcanics of the Ethiopian main Rift, and basement rocks of the Adola Rea, Ethiopia. Mitt Österr Miner Ges, 147, 43-74.

Nath, B. N., Kunzendorf, H., & Pluger, W. L. (2000). Influence of provenance, weathering, and sedimentary processes on the elemental ratios of the fine-grained fraction of the bedload sediments from the Vembanad Lake and the adjoining continental shelf, southwest coast of India. Journal of Sedimentary Research, 70(5), 1081-1094.

Nesbitt HW, Young GM (1982). Early Proterozoic climates and plate motions inferred from the major element chemistry of lutites. Nature 299: 715–717.

Nesbitt HW, Young GM (1984). Prediction of some weathering trends of plutonic and volcanic rocks based on thermodynamic and kinetic considerations. Geochim Cosmochim Ac 48: 1523–1534.

Nichols, G. (2009). Sedimentology and stratigraphy. John Wiley & Sons.

Osae, S., Asiedu, D. K., Banoeng-Yakubo, B., Koeberl, C., & Dampare, S. B. (2006). Provenance and tectonic setting of Late Proterozoic Buem sandstones of southeastern Ghana: Evidence from geochemistry and detrital modes. Journal of African Earth Sciences, 44(1), 85-96.

Pettijohn FJ (1975). Sedimentary Rocks. 2nd ed. New York, NY, USA: Harper and Row.

Pettijohn FJ, Potter PE, Siever R (1972). Sand and Sandstones. 1st ed. New York, NY, USA: Springer-Verlag.

Pettijohn, F. J., Potter, P. E., & Siever, R. (1987). Petrography of Common Sands and Sandstones. In Sand and Sandstone (pp. 139-213). Springer, New York, NY.

Potter, P. E. (1978). Petrology and chemistry of modern big river sands. The Journal of Geology, 86(4), 423-449.

Rollinson HR (1993). Using Geochemical Data: Evaluation, Presentation, Interpretation. London, UK: Longman.

Roser, B. P., & Korsch, R. J. (1986). Determination of tectonic setting of sandstone-mudstone suites using SiO2 content and K2O/Na2O ratio. The Journal of Geology, 94(5), 635-650.

Russo, A., Assefa, G. & Atnafu, B. (1994). Sedimentary evolution of the Abbay River (Blue Nile) Basin, Ethiopia. N. Jb. Geol. Paläont. Mh. 5: 291-308.

Scotese, R. C., & Barrett, S. F. (1990). Gondwana's movement over the South Pole during the Palaeozoic: evidence from lithological indicators of climate. Geological Society, London, Memoirs, 12(1), 75-85.

Sembroni, A., Molin, P., Pazzaglia, F. J., Faccenna, C., & Abebe, B. (2016). Evolution of continental-scale drainage in response to mantle dynamics and surface processes: An example from the Ethiopian Highlands. Geomorphology, 261, 12-29.

Stern, R. J., Johnson, P. R., Kröner, A., & Yibas, B. (2004). Neoproterozoic ophiolites of the Arabian-Nubian shield. Developments in Precambrian Geology, 13, 95-128.

Sun, S. S., & McDonough, W. F. (1989). Chemical and isotopic systematics of oceanic basalts: implications for mantle composition and processes. Geological Society, London, Special Publications, 42(1), 313-345.

Suttner, L. J., & Dutta, P. K. (1986). Alluvial sandstone composition and paleoclimate; I, Framework mineralogy. Journal of Sedimentary Research, 56(3), 329-345.

Tadesse, T., Hoshino, M., Suzuki, K., & Iizumi, S. (2000). Sm, Nd, Rb, Sr and Th, U, Pb zircon ages of syn-and post-tectonic granitoids from the Axum area of northern Ethiopia. Journal of African Earth Sciences, 30(2), 313-327.

Taylor, S.R., McLennan, S.M. (1985). The continental crust: its composition and evolution. Blackwell, Oxford, pp. 312.

Torsvik, T.H., Cocks, L.R.M., 2013. Gondwana from top to base in space and time. Gondwana Research 24, 999-1030.

Tsige L. (2008). Geology of Bure map sheet (NC-37-5). Survey of Ethiopia. Unpublished report.

Verma SP, Armstrong-Altrin JS (2013). New multi-dimensional diagrams for tectonic discrimination of siliciclastic sediments and their application to Precambrian basins. Chem Geol 355: 117-180.

Wedepohl, K.H. (1978). Handbook of Geochemistry, Volume II, Part 2. Springer, Berlin, Heidelberg, New York, pp. 1546.

Wolela, A. (1997). Sedimentology, diagenesis, and hydrocarbon potential of sandstones in hydrocarbon prospective Mesozoic rift basins (Ethiopia, United Kingdom, USA). Unpublished Ph. D. dissertation, Queen's University of Belfast, Belfast, N. Ireland.

Wolela, A. (2007). Source rock potential of the Blue Nile (Abay) basin, Ethiopia. Journal of Petroleum Geology, 30(4), 389-402.

Wopfner, H., & Kreuser, T. (1986). Evidence for Late Palaeozoic glaciation in southern Tanzania. Paleogeography, Palaeoclimatology, Palaeoecology, 56(3-4), 259-275.

Wronkiewicz, D.J., Condie, K.C. (1987). Geochemistry of Archean shales from the Witwatersrand Supergroup, South Africa: Source-area weathering and provenance. Geochimica et Cosmochimica Acta 51, 2401-2416.

Zaid, S. M., & Al Gahtani, F. (2015). Provenance, diagenesis, tectonic setting, and geochemistry of Hawkesbury Sandstone (Middle Triassic), southern Sydney Basin, Australia. Turkish Journal of Earth Sciences, 24(1).

Appendix

Table 2- Locations of the upper Paleozoic sandstones sampling sites and outcrops, with GPS coordinate.

Sample	Location	Northing	Easting	Position	Lithology	color	size	considerable features
Mst1-sen	Sentom	10°23.652	37°01.722	top	mudstone	red	-	Laminated silty mudstone
SST2-bok	Boko Tabo	10°22.163	37°00.827	bottom	sandstone	brown	medium	Soft, friable sandstone
SST3-bok	Boko Tabo	10°22.239	37°00.954	bottom	sandstone	white	coarse	Hard, massive Sandstone wi
SST4-bok	Boko Tabo	10°22.005	37°01.196	bottom	sandstone	Pinkish white	medium	Sandstone with muds
SST5-bok	Boko Tabo	10°23.072	37°01.382	top	sandstone	White	medium	Massive, hard sandstone
SST6-sen	Sentom	10°23.888	37°02.557	top	sandstone	white	fine	Slightly crumbled sandstone
SST8-bok	Boko Tabo	10°22.230	37°00.964	bottom	sandstone	Pale green	medium	Hard Sandstone with speckle
SST9-bok	Boko Tabo	10°22.292	37°00.972	bottom	sandstone	white	coarse	Oxidized sandstone
SST10-sen	Sentom	10°24.382	37°00.772	top	sandstone	red	coarse	Massive sandstone with sec
Sit2-bok	Boko Tabo	10°22.531	37°00.998	middle	siltstone	Dark red	fine	laminated Silty mudstone
Sit5-bok	Boko Tabo	10°22.733	37°00.913	middle	siltstone	white	coarse	Black and white lamination
Sit6-bok	Boko Tabo	10°22.811	37"°01.021	middle	siltstone	red	midium	laminated siltstone
SST1-dag	Daguja	10°18.929	37°02.922	top	sandstone	Pale pink	coarse	Massive, crumbled (soft) sa
SST2-dag	Daguja	10°18.932	37°02.939	top	sandstone	yellow	fine	Massive hard
SST3-dag	Daguja	10°18.692	37°03.132	top	sandstone	brown	medium	Soft sandstone
Sit1-dag	Daguja	10°18.532	37°03.072	top	siltstone	Pale yellow	medium	Hard sandstone
til1-dag	Daguja	10°18.548	37°03.171	middle	tillite	pink	-	

Table 3 Point-counted data and the derived QFL indices of the upper Paleozoic sandstone: zi (zirconium), tou (tourmaline), ru (rutile), gar (garnet), opx (orthopyroxene), hem (hematite), cal (calcite), mosc (muscovite), bio (biotite), sit (siltstone), sst (sandstone), FS (fine size), MS (medium size), CS (coarse size), PS (poorly sorted), MS (moderately sorted), WS (well sorted).

	Quartz (%)			Feldspar (%)				Rock Fragent (%)										
Sample	MQ	PQ	Q-total	M	O	Plg	F-total	SRF	MRF	PIRF	RF-total	total cc	HM	Opq	cement	Roundn	Grain	Sorti
SST2-bok	26.4	44.3	70.7	8.8		19.5	28.3	0.3		0.7	1	307	2zi,1tou,1ru	2	hem,musc,cal	subangular	MS	PS
SST3-bok	42.9	27.2	70.1	6.4	1.9	19.1	27.4	0.8	0.3	_	1.1	357	2tou,1 ru	2	qrtz,hem,cal	subangular	CS	WS
SST4-bok	39.9	23.5	63.4	6.4	0.77	25.6	32.77	0.26	2.8	_	3.06	391	3zi, 2tou	3	cal,hem	angular	MS	PS
SST5-bok	70.8	28.6	99.4	0.3	_	0.3	0.6	_	_	_	_	339	2zi,1tou,2ru	2	sit,sst	subround	MS	MS
SST6-sen	80.7	15.6	96.3	0.3	0.3	_	0.6	_	_	1.3	1.3	301	5zi,3tou,1ru	2	sit	subround	FS	PS
SST8-bok	41.7	23.4	65.1	7.4	0.5	23.7	31.6	0.5	_	_	0.5	393	3zi, 1ru,1tou,1 opx,2gar	2	qr,hem,cal	sub angular	MS	PS
SST9-bok	47.3	20.4	67.7	7.5	0.3	23.2	31	0.3	0.6	_	0.9	319	3zi,2tou,1ru,1gar	3	cal,musc,hem	subangular	CS	MS
SST10-bok	76.1	23.3	99.4	0.3	_	0.3	0.6	_	_	_	_	305	4zi,3tou, 1ru	1	qr,sit,hem,cal	subround	CS	MS
Sit2-bok	50.7	11.1	61.8	3.7	3.4	24.4	31.5	2.3	3.4	_	5.7	353	6tou,1ru	1	cal, hem,bio,musc	angular	FS	PS
Sit5-bok	36.8	20.2	57	5	3	29.5	37.5	_	2.7	_	2.7	302	5zi,2tou	1	musc,he,cal	angular	CS	PS
Sit6-bok	42.5	17.5	60	5.3	1	22	28.3	9.6	1.5	_	11.1	395	5zi,1tou	3	hem,musc,cal	angular	MS	PS
SST1-dag	17.6	31.1	48.7	15.4		26.7	42.1	5.3	3.8		9.1	318	1zi	_	hem,musc	subangular	CS	MS
SST2-dag	21.9	35.3	57.2	11	3.5	22.2	36.7	2.1	4		6.1	374	5zi,3tou1ru	2	cal, hem	subangular	FS	MS
SST3-dag	29.5	30.7	60.2	14.2	1.8	21.1	37.1		2.7		2.7	332	1zi,4tou	_	cal,musc,	subangular	MS	MS
Sit1-dag	24.8	42.6	67.4	6.1	2.9	21.6	30.6		1.9		1.9	310	2zi,3tou,1ru,1opx	4	musc,cal	subangular	MS	PS

Table 4- Major element composition with CIA, CIW and PIA values of Late Palaeozoic sandstones. Element concentrations were measured -AES are given in weight%.

SAMPLE	SiO2	Al2O3	Fe2O3	CaO	MgO	Na2O	K2O	TiO2	MnO	P2O5	Sum	%LOI	CIA	CIW	PIA
SIT1(DAG)	65.3	12.75	3.09	5.94	1.11	4.81	1.73	0.47	0.11	0.17	95.488	4.94	66.1	54.26	57.
SIT5(BOK)	80	11.1	1.22	0.67	0.49	3.19	1.35	0.22	0.01	0.02	98.272	2.84	68.06	74.2	59.
MST1(	74.6	14.05	4.37	0.05	0.14	0.04	0.72	0.75	0.01	0.18	94.918	5.15	94.55	99.36	89
SIT6(BOK)	78.7	11.25	1.98	0.34	0.13	4.14	2.01	0.26	0.05	0.05	98.915	1.22	63.42	71.52	52.
SST1(DAG)	76.5	12.2	1.38	0.42	1.85	1.96	1.01	0.33	0.03	0.04	95.723	4.95	78.26	83.68	71.
SST5(BOK)	96	3	0.41	0.02	0.04	0.01	0.04	0.15	0.01	0.01	99.68	1.23	97.72	99.01	96.
SST3(BOK)	95.1	3.09	0.68	0.09	0.09	0.74	0.53	0.11	0.03	0.01	100.473	0.9	69.44	78.83	57.
TIL1(DAG)	74.8	13.95	1.27	0.66	0.12	4.33	4.1	0.15	0.02	0.05	99.453	0.67	60.55	73.65	42.

Table 5- Trace elements composition of Late Palaeozoic sandstones. Element concentrations were measured with ICP-MS and ICP-AES are given in ppm.

SAMPLE	Ba	Ce	Cr	Cs	Dy	Er	Eu	Ga	Gd	Hf
SIT1(DAG)	608	34.3	40	0.24	4.07	2.8	1.42	11.7	4.64	4.
SIT5(BOK)	727	20.7	10	0.89	1.2	0.77	0.49	9.6	1.47	4.
MST1(	536	104	50	1.17	6.73	3.58	1.96	15.6	8.82	9.
SIT6(BOK)	607	19.5	30	0.31	1.65	1.11	0.68	10.5	2.01	3.
SST1(DAG)	298	47.1	10	0.64	3.1	1.61	1.36	11.4	4.33	6.
SST5(BOK)	22.6	24.5	10	0.09	1.29	0.64	0.44	2.4	1.78	3.
SST3(BOK)	188.5	18.2	10	0.21	0.81	0.51	0.34	2.3	1.16	2.
TIL1(DAG)	914	14.7	10	2.46	1.36	0.88	0.33	13.9	1.24	2.

SAMPLE	Ho	La	Lu	Nb	Nd	Pr	Rb	Sm	Sn	Sr
SIT1(DAG)	0.81	17.7	0.34	5.9	19.6	4.68	34.9	4.37	3	31
SIT5(BOK)	0.24	10.4	0.12	3.4	9.5	2.47	34.2	1.64	2	110
MST1(	1.24	57.2	0.48	15.9	54.9	13.8	28.4	9.81	5	29
SIT6(BOK)	0.36	11.3	0.2	3.5	11.2	2.78	39.6	2.01	2	14
SST1(DAG)	0.6	28.5	0.23	5.7	28.1	7.05	25.5	5.59	2	53
SST5(BOK)	0.24	12.3	0.12	2.9	11.3	3.06	1.5	2.06	2	6.
SST3(BOK)	0.16	9	0.06	1.8	8.6	2.13	11.6	1.63	1	27
TIL1(DAG)	0.28	7.4	0.14	4.8	6.5	1.64	132.5	1.52	1	22

SAMPLE	Ta	Tb	Th	Tm	U	V	W	Y	Yb	Zr
SIT1(DAG)	0.6	0.66	2.28	0.39	1.01	75	2	26.8	2.36	15
SIT5(BOK)	0.3	0.16	2.42	0.12	0.43	13	<1	6.3	0.85	17
MST1(	1.1	1.2	12.7	0.51	2.2	67	3	30.2	3.4	33
SIT6(BOK)	0.4	0.25	2.1	0.18	0.65	38	1	9.8	3.4	12
SST1(DAG)	0.4	0.57	3.35	0.24	0.74	17	1	15.7	3.4	28
SST5(BOK)	0.2	0.22	2.64	0.12	0.6	6	1	6.8	3.4	13
SST3(BOK)	0.3	0.14	1.46	0.08	0.2	12	1	4.1	3.4	8
TIL1(DAG)	0.4	0.18	6.65	0.15	1.52	19	2	8.2	3.4	7

Table 6 - Values of Pearson,s coefficient of correlation of major elements of the studied samples (A) for Bokotabo-Sentom area, (B) for Daguja area.

A

	SiO2	TiO2	Al2O3	P2O5	Fe2O3	K2O	Na2O	CaO	MgO	MnO	Eu/Eu*	(La/Yb)N	(Gd/Yb)N
SiO2	1												
TiO2	-0.73627	1											
Al2O3	-0.99804	0.759916	1										
P2O5	-0.71021	0.99350	0.7299	1									
Fe2O3	-0.8140	0.978656	0.82758	0.4984261	1								
K2O	-0.6750	0.10481	0.16363	0.50528	0.2225122	1							
Na2O	-0.4446	-0.2660	0.140465	-0.2760	-0.105	0.98938276	1						
CaO	-0.4339	0.2190	0.141999	0.2854	-0.1410	0.769550	0.5814287	1					
MgO	-0.4595	-0.0146	0.646564	-0.1010	0.0027	0.444830	0.6531	0.761917079	1				
MnO	-0.0601	-0.284	0.500524	0.20098	0.0976	0.264330	0.360524	0.106920	0.28763	1			
Eu/Eu*	-0.322	-0.3936	0.928249	0.4053	0.241	0.948830	0.699030	0.848165	0.715214	0.4597334	1		
(La/Yb)N	0.58270	0.306038	0.5506	0.707844	-0.076	-0.9212	-0.93	-0.71796	0.44339	0.5196	-0.90782	1	
(Gd/Yb)N	0.39036	0.433022	-0.3544	0.35310	0.1896	-0.88746	-0.98950	-0.8575	-0.5860	-0.5170	-0.9930	0.5932167	1
(La/Sm)N	-0.2500	-0.0370	0.125712	-0.0973	-0.0250	0.921090	0.326270	0.1695	0.68865	-0.3095	0.2575	-0.1986	-0.24

B

	SiO2	TiO2	Al2O3	P2O5	Fe2O3	K2O	Na2O	CaO	MgO	MnO
SiO2	1									
TiO2	-0.74053	1								
Al2O3	0.06989	-0.72214	1							
P2O5	-0.9970	0.478703	-0.1416	1						
Fe2O3	-0.9810	0.185682	-0.262	0.7992434	1					
K2O	0.15709	-0.78	0.02996	-0.2278	-0.34569	1				
Na2O	-0.7330	0.808579	0.362724	-0.68216	-0.5872	0.2556533	1			
CaO	-0.994	0.728055	-0.17	0.99995	0.99957	-0.2576	0.4659394	1		
MgO	0.05800	0.6627	-0.99	0.820140	0.7136	-0.973	-0.7216	0.3044753	1	
MnO	-0.970	0.668039	-0.30	0.7985	0.6599	-0.3899	0.6548	0.9990	0.5183725	1

Table 7 - Values of Pearson,s coefficient of correlation of the selected trace element of the studied samples

	Cs	Rb	Ba	Sr	Th	U	Y	Zr	Hf	Nb	Ta	Sc	Cu	Ni	SREE	SLREE	SHREE
Cs	1																
Rb	0.563737	1															
Ba	0.70194	0.1964581	1														
Sr	0.84671	0.664311	0.4644501	1													
Th	0.76623	0.118441	0.323100	0.5868211	1												
U	0.72103	0.423771	0.325356	0.8890	0.4986112	1											
Y	0.74231	0.929269	0.830161	0.491836	0.498518	0.99531	1										
Zr	0.86749	0.931738	0.639882	0.389387	0.396496	0.395850	0.6951539	1									
Hf	0.86704	0.731041	0.539144	0.889432	0.296928	0.796064	0.795469	0.6999787	1								
Nb	0.78780	0.526056	0.629824	0.390512	0.499673	0.898933	0.799326	0.896930	0.1973096	1							
Ta	0.77422	0.434654	0.835541	0.293503	0.996887	0.396092	0.498234	0.792026	0.692607	0.7981513	1						
Sc	0.76532	0.366326	0.162967	0.998787	0.583100	0.787649	0.590315	0.28532	0.885231	0.787258	0.8905855	1					
Cu	0.853	0.50569	0.854270	0.395910	0.891799	0.194316	0.194570	0.596920	0.96670	0.594060	0.891606	0.2945984	1				
Ni	0.08307	0.685776	0.976318	0.819613	-0.3096	-0.2224	-0.1769	-0.1734	-0.1838	-0.2331	-0.1420	0.226189	0.05324	1			
SREE	0.74624	0.218180	0.221734	0.786922	0.199858	0.998561	0.898769	0.9510	0.95666	0.399606	0.497620	0.583476	0.9081	-0.30895	1		
SLREE	0.74494	0.1742	0.82111	0.286527	0.9986	0.19845	0.298628	0.695077	0.695590	0.499540	0.597490	0.182992	0.9051	-0.3169	0.99996	1	
SHREE	0.75840	0.229056	0.930640	0.191910	0.298906	0.499290	0.599923	0.695490	0.295856	0.199640	0.298680	0.889810	0.994352	-0.1880	0.199136	0.5990154	1

Table 8- Selected ratios for the upper Paleozoic sandstones

SAMPLE	SREE	SLREE	SHREE	SLREE/SHREE	Eu/Eu*	(La/Yb)N	(La/Sm)N	(Gd/Y
SIT5(BOK)	50.1	46.7	3.5	13.5	1.0	8.3	4.0	1.
MST1(	267.6	250.5	17.1	14.6	0.6	11.4	3.7	2.
SIT6(BOK)	54.5	49.5	5.0	9.9	1.0	6.2	3.5	1.
SST3(BOK)	43.3	41.1	2.2	18.3	0.8	12.7	3.5	2.
SST5(BOK)	58.8	55.4	3.4	16.5	0.7	11.5	3.8	2.
SIT1(DAG)	94.9	83.5	11.4	7.3	1.7	5.1	2.5	0.
SST1(DAG)	129.9	122.0	7.9	15.5	0.8	12.6	3.2	2.
TIL1(DAG)	37.2	33.3	3.9	8.6	0.7	5.6	3.1	1.

Table 9 - Linear correlation coefficients for selected element distribution in the analyzed samples (A) for Bolotabo„ Sentom area, (B) for Daguja area

Selected element (A)	correlation coe	Selected element (B)	correlation coe
TiO_2- Zr	0.972	TiO_2- Zr	0.44308
TiO_2-Th	0.985	TiO_2-Th	-0.977
TiO_2-Sc	0.934	TiO_2-Sc	0.827
TiO_2ΣREE	0.925	TiO_2ΣREE	0.67148
Al_2O_3-V	0.575	Al_2O_3-V	-0.17988
Al_2O_3- La	0.419	Al_2O_3- La	-0.97481
Al_2O_3- Yb	-0.17	Al_2O_3- Yb	0.03759
Al_2O_3ΣREE	0.43	Al_2O_3ΣREE	-0.99750
Al_2O_3 -Th	0.64	Al_2O_3 -Th	0.85
Al_2O_3-Sc	0.879	Al_2O_3-Sc	-0.209
Al_2O_3-Cs	0.763	Al_2O_3-Cs	0.885
Al_2O_3-Rb	0.794	Al_2O_3-Rb	0.972
Al_2O_3-Sr	0.870	Al_2O_3-Sr	0.482
Al_2O_3-Ba	0.821	Al_2O_3-Ba	0.976
P_2O_5ΣREE	0.73	P_2O_5ΣREE	0.07133
Zr- La	0.908	Zr- La	0.99245
Zr- Yb	0.024	Zr- Yb	0.13618
Cr- V	0.954	Cr- V	0.99953
Th-Nb	0.918	Th-Nb	-0.997